New Mass and Orbital constraints of J1407b

Bharath Chowdhary Nagam

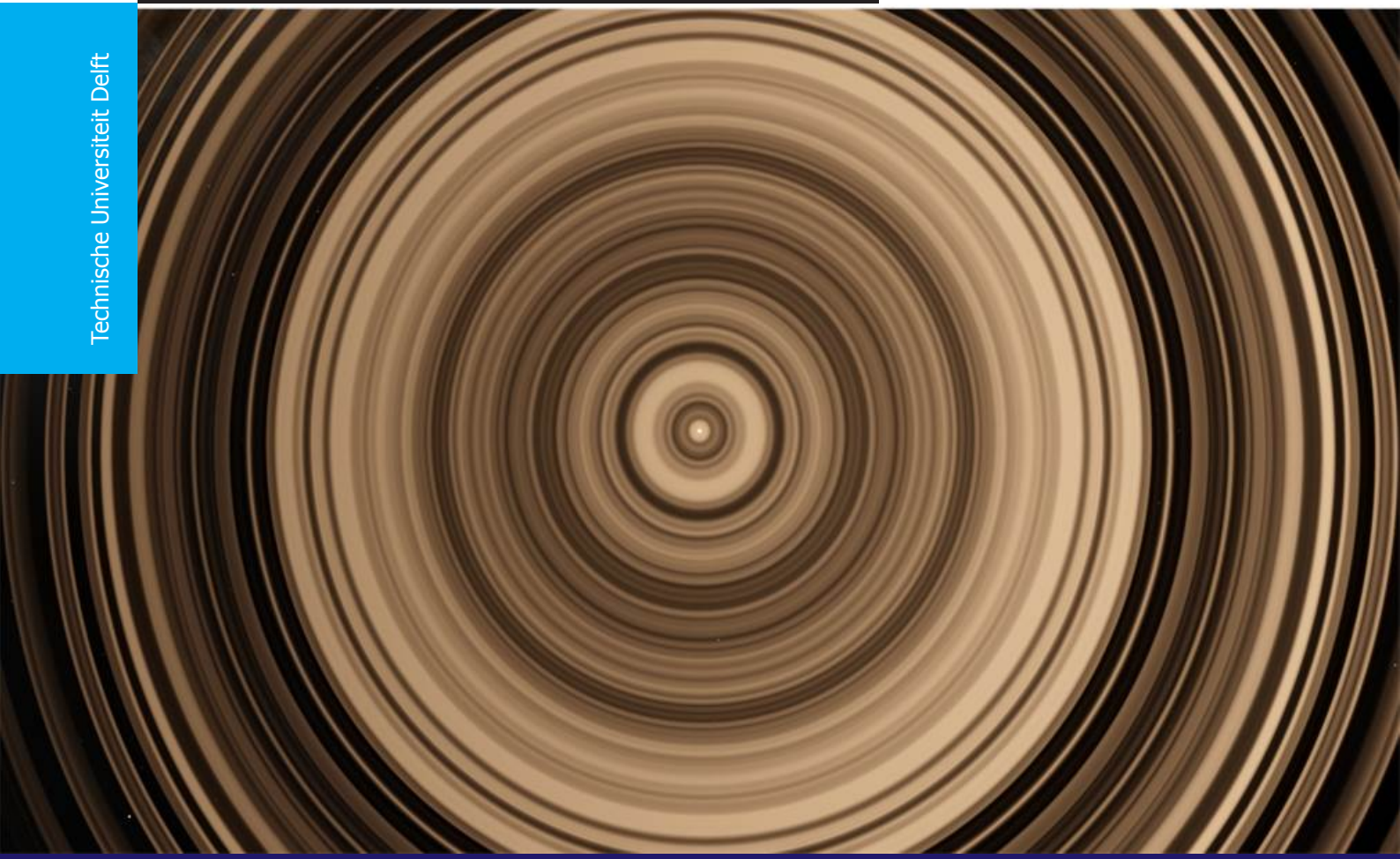

Technische Universiteit Delft

TU Delft Delft University of Technology

Challenge the future

New constraints on mass and orbital parameters of J1407b

by

Bharath Chowdhary Nagam

in partial fulfillment of the requirements for the degree of

Master of Science

in Aerospace Engineering

at the Delft University of Technology,

to be defended publicly on Monday July 24, 2017 at 2:00 PM.

Supervisor:	Dr. Matthew Kenworthy(external)	
	Dr. Daphne Stam(internal)	
Thesis committee:		
	Ir. Prem Sundaramoorthy,	TU Delft
	Samiksha Mestry M.Eng,	TU Delft

This thesis is confidential and cannot be made public until July 24, 2017.

TU Delft Delft University of Technology

Acknowledgement

First and foremost, I thank the Almighty for giving me the strength, knowledge and opportunity to undertake this research and complete it satisfactorily.

I sincerely thank Dr.Daphne Stam of TU Delft, who gave me this opportunity and referred me to Dr.Matthew Kenworthy of Leiden University. I also thank her for her numerous suggestions and insightful inputs in the end to make this thesis report more meaningful and attractive to read.

I also sincerely thank Dr.Matthew Kenworthy, who , in spite of his very busy schedule, solely guided me in completion of this project. His advice and teachings will not only help me in just completing this course, but also for my entire career.

I thank my Parents, who have supported me throughout my life to successfully become a graduate and a professional.

Lastly, my friends in Delft , who provided me with great moral support and helped me in various difficult situations throughout my master's.

Thanks for all your encouragement and support!

Bharath Chowdhary Nagam

Delft, July 2017

Contents

List of Figures vii

List of Tables xi

1 Abstract 1

2 Introduction 3

2.1 Introduction to Exoplanets . . . 3

2.2 J1407b-An exoplanet with giant ring system . . . 4

2.3 Overview . . . 10

3 Earlier research on J1407 and its companion 13

3.1 About the star-J1407 . . . 13

3.2 Light Curve . . . 14

3.3 Possible explanations for the eclipse . . . 15

3.4 Modelling of the ring system . . . 16

3.5 Orbital Constraints. . . . 19

3.5.1 Direct Imaging . . . 19

3.5.2 Photometry . . . 20

3.5.3 Radial Velocity . . . 20

3.5.4 ξ constraint . . . 21

3.5.5 Eccentricity Limit. . . . 21

3.5.6 Mass and Period Limits . . . 24

3.6 Conclusion . . . 25

4 Introduction to Orbital Parameters and Observation Techniques 27

4.1 Definition of Orbital Parameters . . . 27

4.2 Visualisation of orbital parameters . . . 28

4.2.1 visualisation of inclination(i) . . . 28

4.2.2 visualisation of Ω . . . 28

4.2.3 visualisation of ω . . . 31

4.3 Development of Algorithm . . . 31
4.4 Introduction to Direct Imaging . . . 35
4.5 Introduction to Transit photometry . . . 36
4.5.1 Importance of photometry . . . 37
4.6 Introduction to Radial Velocity(RV) . . . 38
4.7 Conclusion . . . 39

5 Inclination and Eccentricity Constraint **41**
5.1 Introduction . . . 41
5.2 Eccentricity Constraints . . . 41
5.3 Inclination constraint . . . 43
5.4 Conclusion . . . 43

6 Direct Imaging **45**
6.1 Observations of J1407 . . . 45
6.2 Conclusion . . . 49

7 Photometry **51**
7.1 Photometry data of J1407 . . . 51
7.2 Conclusion . . . 53

8 Radial Velocity **57**
8.1 Radial Velocity data of J1407 . . . 57
8.2 Constraints for Circular Orbit . . . 57
8.3 Constraints for Elliptical Orbit . . . 59
8.4 Conclusion . . . 59

9 Results and Conclusion **63**
9.1 Combined constraints for circular orbits . . . 63
9.2 Combined constraints for elliptical orbits . . . 63
9.3 Result . . . 65
9.4 Conclusion . . . 65

10 Recommendations **69**

11 Appendix **71**
11.1 Appendix-a . . . 71
11.2 Appendix-b . . . 71

Bibliography **75**

List of Figures

2.1 **Habitable zone of recently discovered exoplanets[1]** 4
2.2 **Transit Method[2]** 5
2.3 **Dip in brightness flux of J1407[3]** 5
2.4 J1407b (described by black circle) and its ring system described in series of colors of brown,cyan,blue,orange,gray, if present at the centre of earth-sun system , will tend to fill the entire gap between earth(yellow circle) and sun(red circle) and will even tend to extend beyond. 6
2.5 **Rings of J1407b [4]** 7
2.6 **Transit curve showing successive dips of flux in the HAT-P7 system[5]** . . . 7
2.7 **Change in Radial Velocity of the star due to the gravitational tug of companion[6]** 8
2.8 **Direct imaging of an exoplanet orbiting the star 1RXS J160929.1 – 210524 [7]** 9
2.9 **Number of Exoplanets detected by various methods[8]** 9

3.1 **CTIO spectra of four standard stars[9]** 14
3.2 **superWASP photometry light curve of J1407[9]** 15
3.3 **ASAS photometry light curve of J1407[9]** 15
3.4 **A basic ring model to fit superWASP data[9]** 16
3.5 **Geometry of the ring model[3]** 17
3.6 **Ring model fit to the data[3]** 18
3.7 **Simulation of prograde and retrograde models[10]** 18
3.8 **Eclipse duration for different models[10]** 18
3.9 **RV data of J1407[11]** 21
3.10 **period and mass limits for circular orbit of J1407b[11]** 22
3.11 **period and mass limits for elliptical orbit of J1407b[11]** 23
3.12 **Combined period and mass limits for circular orbit of J1407b[11]** 24
3.13 **Combined period and mass limits for elliptical orbit of J1407b[11]** 25

4.1 **Plot describing inclination(i) of arbitrary companion in the plane of sky** . . . 29
4.2 **Plot describing Ω of arbitrary companion in the plane of sky** 30
4.3 **Plot describing ω** 32
4.4 **Plot describing function of ω** 33

4.5 **Position coordinates in the sky** . . . 34
4.6 **Direct Imaging of HR8799 system[12]** . . . 36
4.7 **Integrated image showing the path of Venus transit[13]** . . . 37
4.8 **Illustration of a transit curve[14]** . . . 37
4.9 **Plot describing the change in Radial Velocity of a star versus time [15]** . . . 39

5.1 **Eccentricity values satisfying the velocity constraint** . . . 42
5.2 **Critical eccentricity values from Kenworthy et al.(2015)[11]** . . . 42
5.3 **Critical inclination values which satisfies the modelled value of impact parameter** . . . 44

6.1 **Constraints for circular orbit of J1407b[11]** . . . 46
6.2 **Direct imaging constraint of J1407b(circular orbit)** . . . 47
6.3 **Position of Secondary Companion during various epochs of direct imaging** . . . 48
6.4 **Direct Imaging constraints for elliptical orbits** . . . 50

7.1 **3.2 days phase folded results from van Werkhoven et al.(2014)[16]** . . . 52
7.2 **3.2 day period folding result for transit data of J1407b** . . . 52
7.3 **Photometry constraints of J1407b** . . . 53
7.4 **Photometry data of PDS 110[17]** . . . 53
7.5 **superWASP photometry light curve of J1407[9]** . . . 54
7.6 **Transit light curve of J1407 for the past 5 years[18]** . . . 55

8.1 (a) represents the variation of RV of J1407 with time. (b) represents the FWHM of the star implying heavy stellar activity. (c) representing slope of bisector also is inline with the FWHM, implying high stellar activity. (d) represents the RV vs slope of bisector plot showing very high anti correlation. . . . 58
8.2 **RV Constraints for circular orbit** . . . 59
8.3 **RV Constraints for elliptical orbit from Kenworthy et al(2015)[11]** . . . 60
8.4 **updated RV Constraints for elliptical orbit from the latest data of CORALIE observation** . . . 61

9.1 **Combined constraints for circular orbits** . . . 64
9.2 Combined constraints of RV, DI and photometry for elliptical orbits. The Mean mass for each case of ω(in increasing order) are 7.32,9.10,9.56,10.04,10.43,1.74,14.48 and 24.98 Jupiter masses respectively. . . . 67

11.1 **RV constraint for circular orbits[11]** . . . 72
11.2 **RV constraint result** $\omega = 90$ **and n=9** . . . 72
11.3 **RV constraint result** $\omega = 270$ **and n=11** . . . 72

11.4 **Direct imaging result for circular orbits** 73
11.5 **Direct imaging constraint[11]** 73

List of Tables

3.1 **Stellar Properties of J1407[9]** 14
3.2 **Disk model parameters[3]** 17

9.1 **Mean mass of J1407b for different cases of ω** 64

1

Abstract

Objective: The main objective of this research study is to combine the constraints from the value of impact parameter, transit, direct imaging and the radial velocity data to yield the final constraint of the mass and period of J1407b.

Inclination constraints:In the previous research work of J1407 (kenworthy et al.(2015)[11]), it has been assumed that the orbit of J1407b is edge on($i = 90°$). However, since the impact parameter of J1407b is known from the modelling of the ring system (Kenworthy and Mamajek(2014)[3]), we use the modelled value of impact parameter to find the value of inclination as function of mass and period of J1407b for different values of argument of periastron.

Combination of constraints : New data from Radial Velocity, Direct Imaging and Transit technique are combined to yield the final result of this research work as constraint limit for mass and period of J1407b for different values of argument of periastron.

Result: The maximum mass of J1407b is limited to 63.5 Jupiter masses(M_{Jup}) for all probable cases of argument of periastron.A table containing average expected value of mass of secondary companion for each case of argument of periastron is also presented.

Recommendation: Out of all the exoplanet detection techniques, another set of observation by direct imaging technique will provide the most useful constraint in constraining further the mass limit of J1407b and ruling out the higher orbital period values. Use of Gaussian Process(GP) is strongly recommended for the RV data to remove the effectsf of stellar noise. It is also recommended to

observe the close proximity of the star with sub millimeter wavelengths in order to locate the rings of J1407b, in case of it not being bound to the gravitational tug of J1407.

2

Introduction

This chapter provides an actual overview of research question involved in our thesis with a brief introduction to the previous research work carried out in the same research area and how the problem is solved. Also overview of this research study , are also briefed to explain the reader what he might expect in reading the entire course of this research project.

2.1. Introduction to Exoplanets

Exoplanets are planets revolving the star other than out sun. Exoplanet around a normal star named 51 Pegasi, were the first to be found by Mayor and Queloz([19]) in the year 1995. Since then approximately 4000 exoplanet candidates have been found by various exoplanet detection techniques which are discussed in detail in this chapter later. The research studies about exoplanets are very interesting since it will lead to a possible discovery of 'Intelligent life' in future. Not only the radius and mass of the exoplanet can be detected, but it is also possible to learn more about the atmosphere of exoplanets by studying the light passed through the top layers of atmosphere of the respective exoplanet. Thus it is very fascinating that it is possible to learn about the density, atmosphere and other aspects of a planet that can even be possibly thousands of light years away. Very important aspect of exoplanets is to find whether it can support life or not. To define this, astronomers use a term called as 'Goldilock Zone' or in simpler terms habitable zone, where an exoplanet can possibly support life, based on the amount of radiation it receives from the parent star and the composition of atmosphere to maintain the temperature of the orbiting planet.

Figure 2.1 represents the habitable zones for recently discovered exoplanets by Kepler space telescope(NASA). It represents the energy received by the planet for different surface temperatures

Figure 2.1: Habitable zone of recently discovered exoplanets[1]

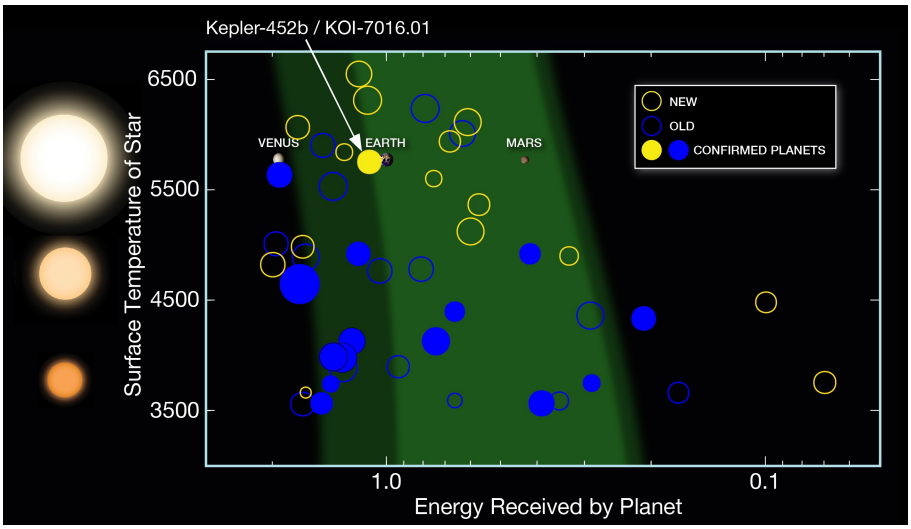

of the star. Green zone represents the habitable zone where the planet receives the right amount of radiation from its parent star to retain any from of life. It is also clear from the figure that Venus is just outside the habitable zone as it receives higher radiation being closer to the sun. The unfilled yellow circles represent the newly discovered Kepler candidates by transit method in which most of the candidates are within the habitable zone.

2.2. J1407b-An exoplanet with giant ring system

J1407 is a young star, located in the southern hemisphere of our sky, which is situated at a distance of 430 light years away from earth. On April 2007, the star showed a huge dip in its brightness which lasted for several weeks. Astronomers call this type of observation as transit data. From the **Figure 2.2**, it is clear that, when a planet or any astronomical object blocks the distant star, a proportional dip in its brightness is observed. Usually this drop in flux is observed for few hours or even to few days. But, J1407 showed a deep eclipse lasting several weeks as shown in the **Figure 2.3**. From the dip in the light curve, it is clear that the pattern is highly asymmetric and complex. Hence, research by Mamajek at al[9], proposed that, the change in brightness of the star might be caused due to the large ring system of the companion object passing in front of the star. This unseen secondary companion has been named J1407b. It is referred to as 'secondary' or 'secondary companion' and not as planet because we do not know the mass of it. Thus it can be either a brown dwarf(a sub stellar object having mass between 13 and 80 Jupiter masses(M_J)) or a planet(having mass less than 13 M_J). Later Kenworthy and Mamajek(2014)[3] modelled the ring system and their ring model consisted of several layers of rings and the diameter of rings extending up to 1.2 AU, i.e., if J1407b is present in between our earth and sun, its ring system will fill the entire gap(between sun and earth) and even extend beyond.

This is explained in the **Figure 2.4**,where Sun(red circle), magnified 10 times, is placed on the centre of the coordinate system and Earth(yellow circle , magnified 500 times) is placed at a distance of 1 AU from the Sun. It is clear form the figure that if J1407b(black circle, maginified as 50 times the size of Jupiter) and its ring system(shown with brown, magenta, blue, orange,cyan and gray rings), placed at the centre of the Earth-Sun system , will fill the entire system and extend beyond. An artist's impression of the rings of J1407b is shown in the **Figure 2.5**.

Figure 2.2: Transit Method[2]

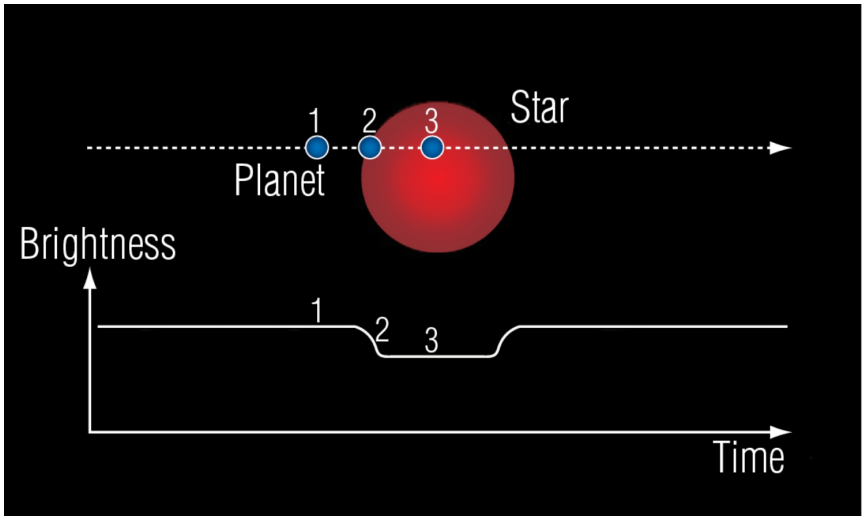

Figure 2.3: Dip in brightness flux of J1407[3]

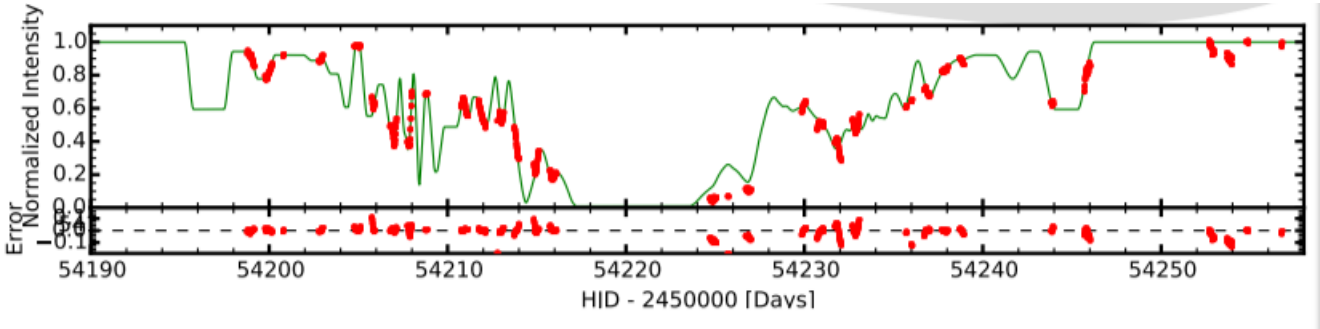

The period of J1407b is unknown. For example, **Figure 2.6** shows the successive transits of the HAT-P7 system. Thus from the figure we know that the period of the companion orbiting the HAT-P7 system is approximately 2 days since the second dip(in Figure 2.6 (a)) is caused after 2 days from the first dip in flux. But for our system in consideration, J1407, has shown only one eclipse(dip in flux) since 2007 and hence the period of J1407b is unknown. The period of J1407b is very important, since it can give the much needed information regarding the next duration of eclipse.

Astronomers use a technique called as Radial Velocity(RV) measurements to measure the mass of the secondary companion. The star and its companion play a tug of war around their common centre

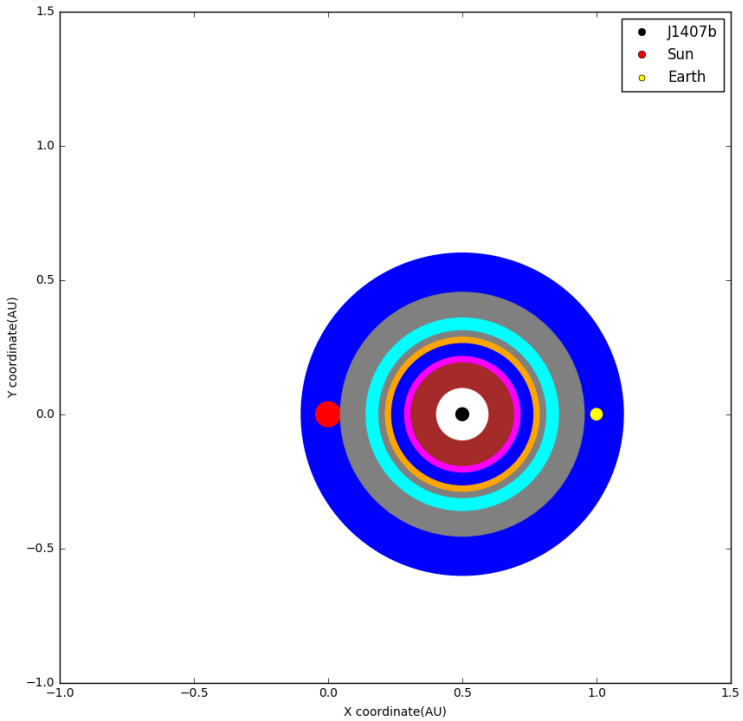

Figure 2.4: J1407b (described by black circle) and its ring system described in series of colors of brown,cyan,blue,orange,gray, if present at the centre of earth-sun system , will tend to fill the entire gap between earth(yellow circle) and sun(red circle) and will even tend to extend beyond.

of mass. **Figure 2.7** clearly explains the change in wavelength of the star light due to the motion of the star caused by the gravitational tug from the companion object. From the rate of change of wavelength, we measure the mass of the secondary companion. However, J1407 is a young star and it produces lot of stellar activity. Stellar activity implies presence of cooler dark spots in the surface of the star. These star spots greatly interfere with the change in wavelength of light and hence RV measurements will be filled with noise. Thus, the mass of J1407b is also unknown. From the mass of J1407b, its hill sphere(a region where gravity of J1407b dominates over its parent star) can be calculated, which in turn will provide interesting conclusion regarding the size of the disk the secondary companion can retain. Thus, finding the mass of secondary companion is crucial in understanding the entire system of J1407b as a whole.

Finally researchers tried to detect J1407b with the help of direct imaging. Direct Imaging is a technique by which the star light is blocked and its close proximity is observed to find the presence of any companion reflecting its star light.For example, **Figure 2.8** shows an star,1RXS J160929.1 − 210524[20], being directly imaged to find a companion(small yellow sphere indicated by red circle) orbiting at a distance of 330 AU from its parent star. Similarly, J1407 was also observed to find any presence of its companion J1407b. But, it resulted in vain.

Figure 2.9 shows the number of exoplanets detected year wise. It is clear from the figure that

Figure 2.5: Rings of J1407b [4]

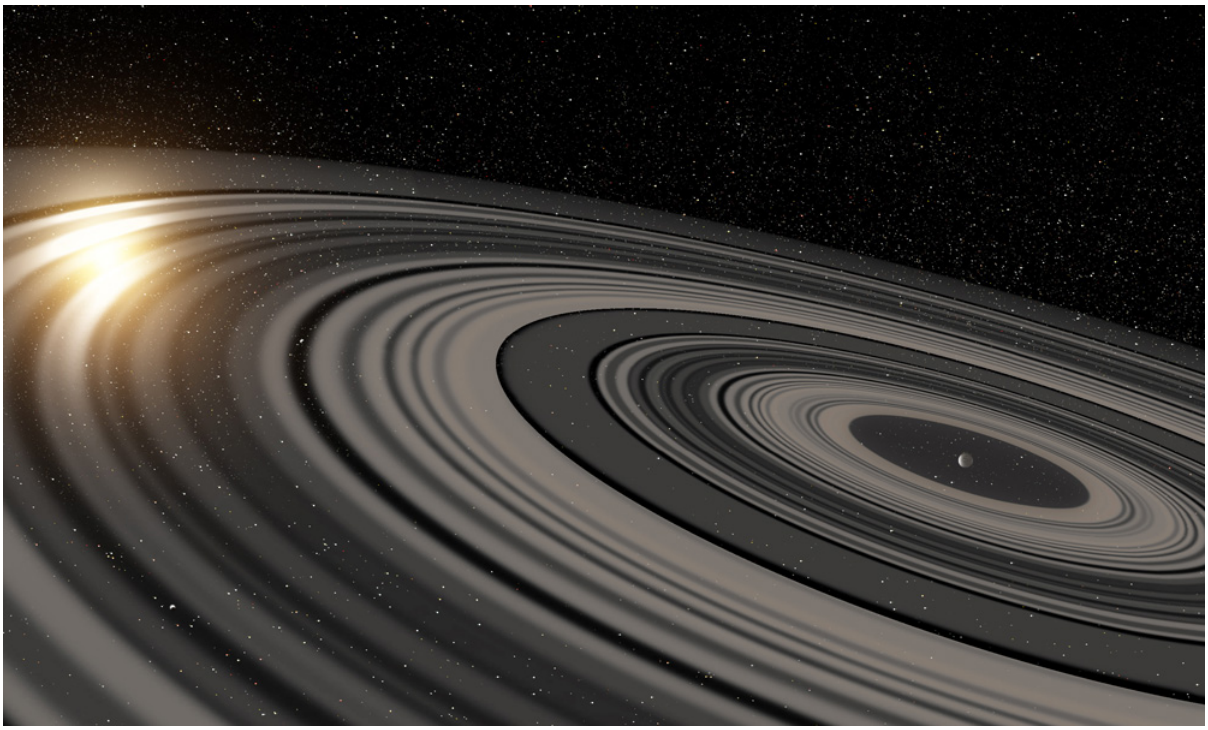

Figure 2.6: Transit curve showing successive dips of flux in the HAT-P7 system[5]

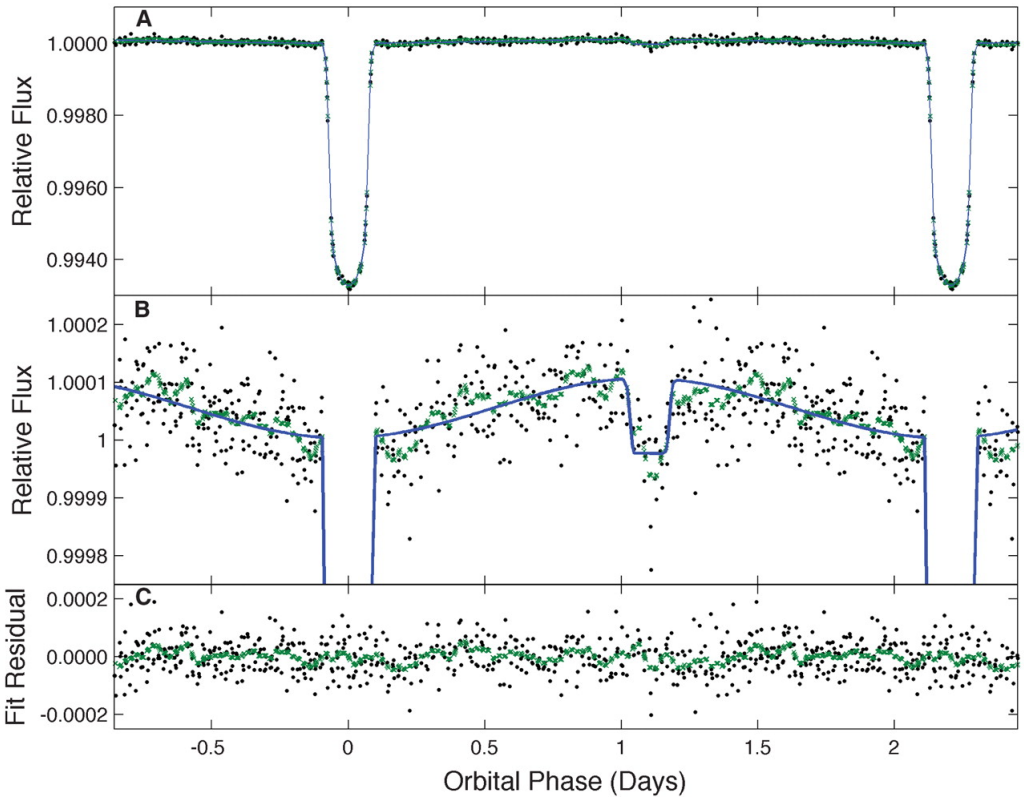

Figure 2.7: Change in Radial Velocity of the star due to the gravitational tug of companion[6]

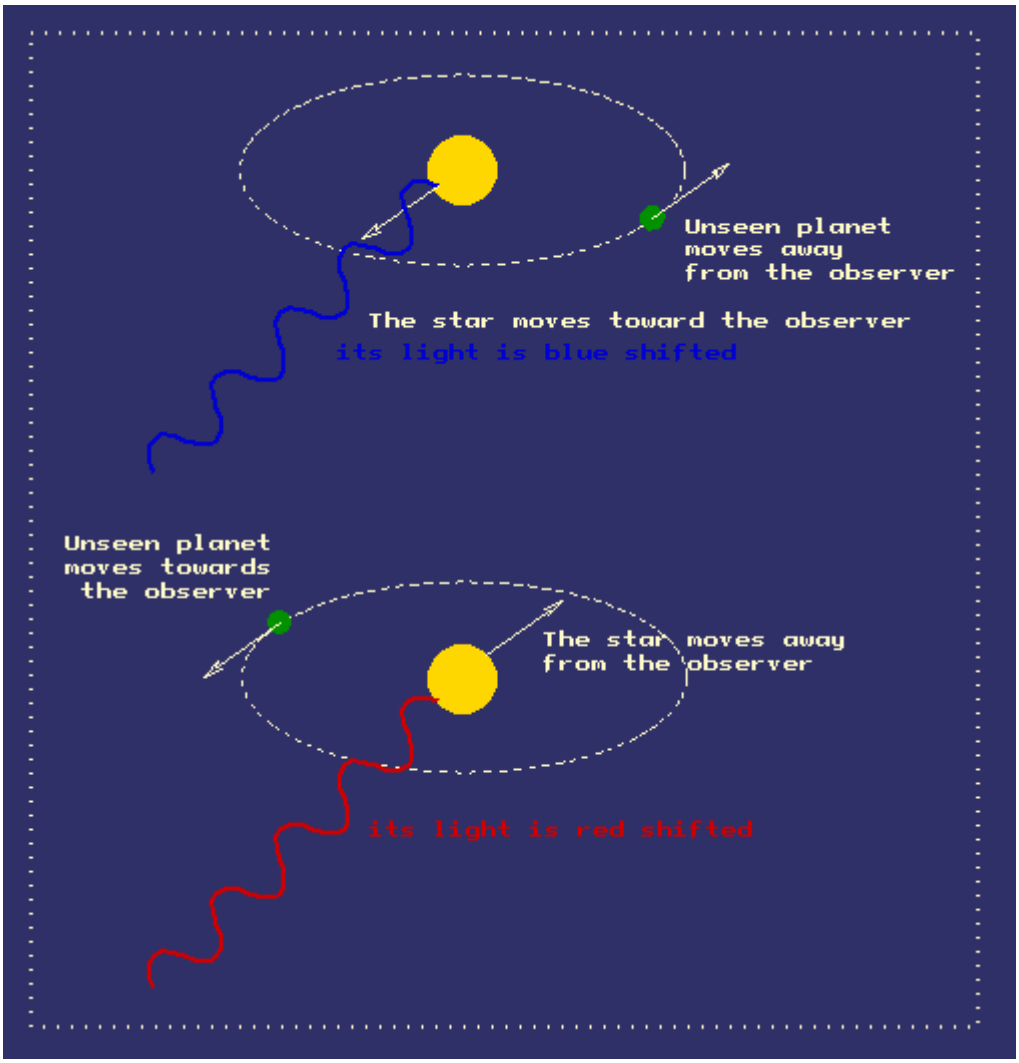

exoplanets are discovered by transit method outnumbers the other methods easily. The reason being, it is very simple to analyse the transit data plots. They are mostly considered noise free when compared to other methods. Radial Velocity(RV) data can be filled with noise if the star is young and lots of stellar activity is taking place. J1407 itself has lot of noise with the RV data since it is very young and its age being only 16 Myr. Direct imaging data is also very difficult to interpret since the star light produces complex interference pattern with the lens of telescope making it highly impossible to detect planets that are very close to the star system. A good example is recently discovered Trappist-1 system[21] in which seven planets were discovered with the help of transit curves. All the seven planets of the system are within 0.06 AU of the star making it highly impossible to detect with direct imaging.

Thus, the period and mass of the secondary companion is unknown. The next step is to find the solution to orbital parameters. Inclination is defined as the angle between the plane of the sky and the orbital plane of the companion. Since, we have seen only the disk of the companion, we know that

Figure 2.8: Direct imaging of an exoplanet orbiting the star 1RXS J160929.1 – 210524 [7]

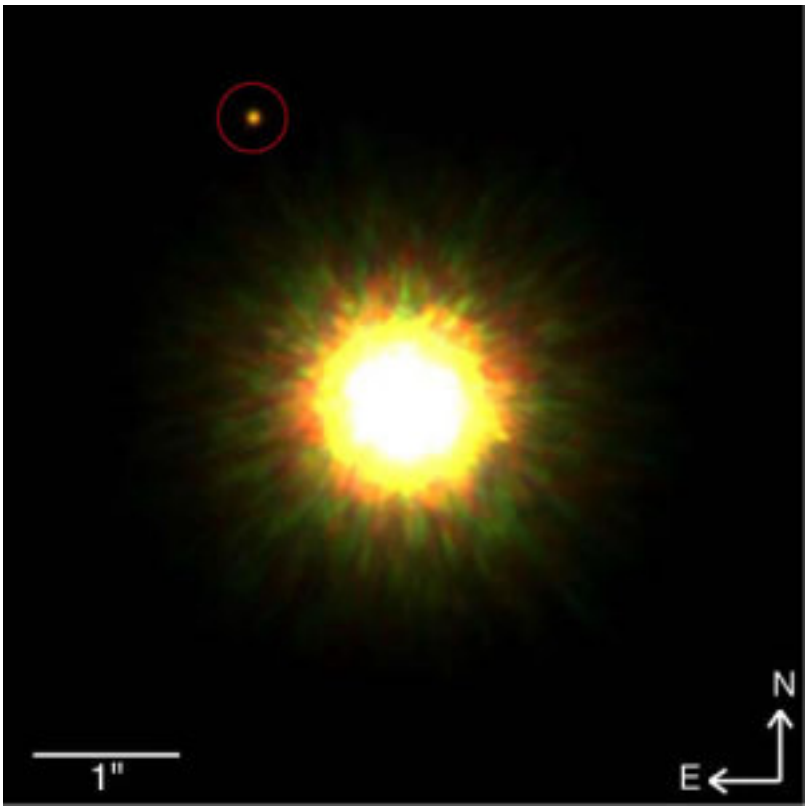

Figure 2.9: Number of Exoplanets detected by various methods[8]

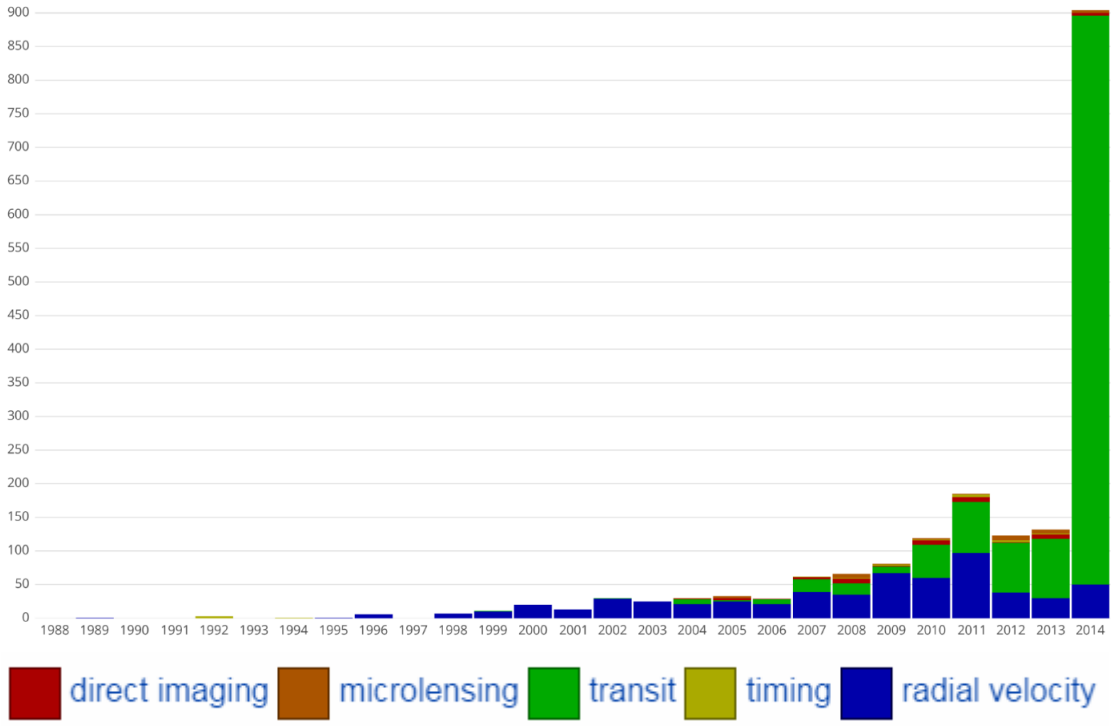

the orbit of J1407b is nearly edge on. However we do not know the exact value of inclination. Impact parameter, defined as the vertical separation of the centre of secondary from the centre of star at the point of closest alignment in the plane of , for J1407b is modelled from the transit data by Kenworthy and Mamajek(2014)[3]. Thus from the value of known impact parameter, the value of inclination can be calculated.

Similarly, from the slopes of transit data of J1407b, van Werkhoven et al.(2014) proposed that the velocity of J1407b at the date of observation was about $32 \pm 2\ kms^{-1}$. For this high velocity, it is proposed that the secondary is most likely to have a highly elliptical orbit(Kenworthy et al.(2015)[11]) and it must have been at (or very close to) its periastron at the eclipse of 2007, i.e., periastron is most likely facing us. It is also important to note that for the previous research work by Kenworthy et al.(2015)[11], they have assumed the inclination to be exactly edge on and direction of periastron to be exactly facing us. So, we have a clue regarding the inclination of the orbit and the orientation of the orbit of J1407b, but it is important to find the exact solution based on the observational data.

Thus, the problem is clear from the introduction. We know that a companion with huge ring system has blocked the light from the star J1407. But it has not been detected by any of the methods and hence its mass and orbital periods are unknown. Thus it is important to constrain the mass and orbital solution of J1407b. We also are yet to find the exact value of inclination and the orientation of the orbit of J1407b. Thus it is also crucial to find the values of these parameters which will be the core part of this thesis.

2.3. Overview

Chapter 3 provides a detailed insight and literature review of the previous research work carried in the J1407 system.

Clear insight into the meaning of orbital parameters is necessary before proceeding with the result of the research. Hence, **Chapter 4** provides clear insight regarding the definition and visualisation of the orbital parameters. A detailed explanation of different exoplanet detection techniques, their advantages and disadvantages have also been explained. Also, brief insight regarding the algorithm developed for conducting this research have also been explained.

The value of impact parameter found by the earlier research studies have implied that the value of inclination cannot be edge on and hence the value of inclination of the secondary has to be calculated for different possible values of argument of periastron which is explained in detail in **Chapter 5**. Circular orbits are highly improbable because of the observed transverse velocity. Hence, it will be a tedious task for both the writer and the reader to include and interpret all the values of eccentricity between 0 and 0.99 to explain the results. Hence, an innovative technique is developed where critical values of eccentricity are derived and verified with earlier results, which are explained in detail in the same chapter.

Chapter 6 explains about constraining the direct imaging data of J1407. In the previous research papers, only constraints based on two epochs of direct imaging were available. Thus, I have calculated the results and constraints of the third epoch of direct imaging and have explained about its importance in the chapter.

In **Chapter 7** , new results from the latest data of the photometry has been included and it has been explained in the chapter about the usefulness of the transit data to rule out different orbital periods. I have also reiterated that the new data also still shows the signs of stellar activity in the chapter.

Chapter 8 explains about the results obtained from the radial velocity data and also the methods that are used to interpret the results. In **Chapter 9** , results and conclusions from all the constraints produced are combined into a single final constraint set to yield some valuable insight about the period and mass of the secondary companion. Also, recommendations and suggestions regarding future plans and observations to be carried out, are presented in **Chapter 10**.

Verification of the algorithm and the results have been explained in **Chapter 11**.

3

Earlier research on J1407 and its companion

In this chapter , earlier research about J1407 and the published results will be studied in detail.

3.1. About the star-J1407

The Spectral class O and B type stars are believed to be evolved from the same molecular cloud and have begin to drift apart. The nearest of OB associations is the Scorpius-Centaurus(Sco-Cen) Association[22]. Spectroscopic survey were conducted for the Sco-Cen for the low mass stars and the results were listed in Pecaut and Mamajek et al(2012)[23]. Among the Sco-Cen members a peculiar light curve was observed for the star 1SWASP J140747.93-394542.6, shortly called as J1407. The peculiar light curve consisted of a rotational variability of 3.2 days caused by the star spots showing that the signs of an young active star and also a deep eclipse which will be discussed in the later section. The numbers '140747.93' and '394542.6' represent the right ascension of $14^h\ 07^m\ 47.93^s$ and declination of $39^\circ\ 45'\ 42.6''$ in J2000 coordinate system respectively[24]. The properties of the star is listed in the **Table 3.1** below

J1407 is classified as a class IV luminosity star from the results obtained from the CTIO spectrograph . From the **Figure 3.1** , it is evident that star J1407, is rich in Lithium with negligible emission of Hα. Since the sodium(Na) feature in the spectrum is weaker when compared to the optical spectrum of the dwarfs and also not in line with that of the giant stars, an intermediate luminosity class of IV is adopted as stated in the research paper by Keenan and McNeil (1989)[25].

Table 3.1: Stellar Properties of J1407[9]

Property	Value
T_{eff}	4500 $^{+100}_{-200}$ K
$\log(\frac{L}{L_\odot})$	-0.47 0.11 dex
Radius(R)	0.96 0.15 $R_\odot$
P_{rot}	3.20 days
Age	16 Myr
Mass	0.9 $M_\odot$

Figure 3.1: CTIO spectra of four standard stars[9]

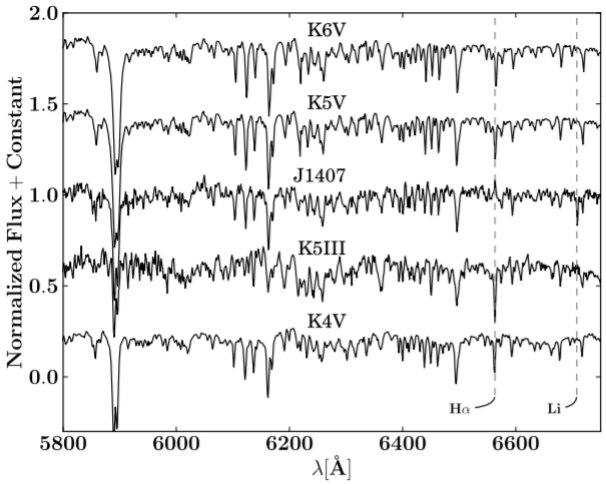

Since the star is from the Upper Centaurus-Lupus(UCL) group of the Sco-Cen Association, the kinematic distance of the star is taken to be 133 $\pm$ 12 pc[3] with a proper motion of 0.9 ±1.8 kms^{-1} .

3.2. Light Curve

superWASP is United Kingdom's leader in the exoplanet survey and detection program. superWASP programme can cover more than 300 degrees of the sky with the telescopes being mounted in both northern and southern hemisphere[26]. The superWASP light curve for the J147 showed deep and long eclipses during April 2007. The photometric data plotted against the time is represented in the **Figure 3.2** . This photometric analysis was also consistent with the light curve obtained from ASAS(All Sky Automated Survey) whose results have been included in the **Figure 3.3**, which also confirms the presence of deep eclipse centered at HJD 2454220.5 days.

The Research by Mamajek et al.(2012)[9] also proved that the light curve has a periodicity of 3.211 days and the result was also in order with the activity of the typical young stars (with J1407 being only 16 Myr old) and in accordance with the results published in Mamajek and Hillenbrand (2008)

Figure 3.2: superWASP photometry light curve of J1407[9]

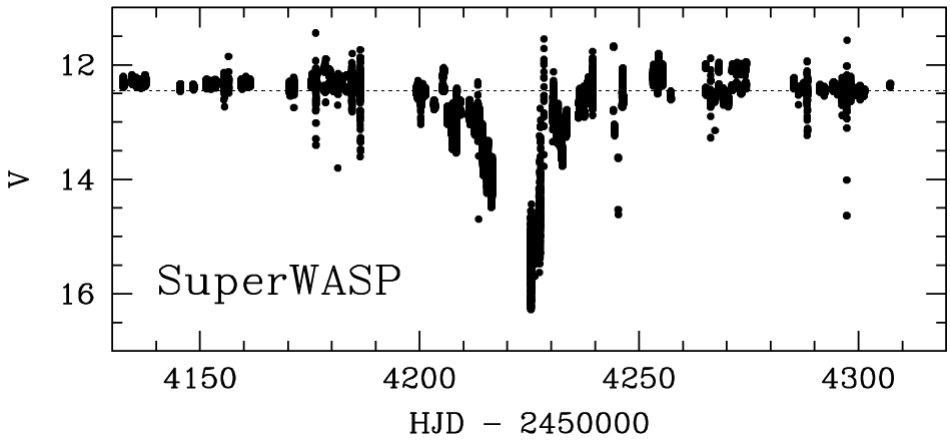

Figure 3.3: ASAS photometry light curve of J1407[9]

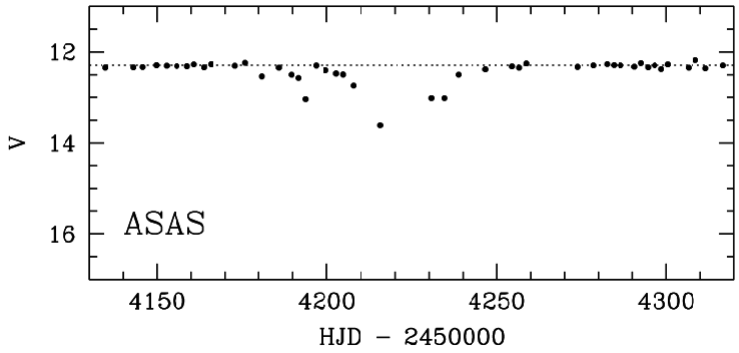

[27].

3.3. Possible explanations for the eclipse

Possible explanations for the eclipse has been explained by Mamajek et al(2012) [9] which has been discussed in detail in this section

- *Eclipse due to secondary companion alone*: Eclipse due to a secondary companion will result in a symmetrical shape and also no secondary companion can cause depth greater than 3 mag.
- *Primary being a red giant which is eclipsing a fainter star*: The infrared emission does not support this hypothesis and hence it is safe to assume that the J1407 is a evolved K5 type star.
- *Eclipse due to presence of disk around a compact stellar remnant*: The star system is very young to possess a neutron star or white dwarf. Also for a blackhole to be present, the X-ray emission should be stronger($L_x > 10^{32}$ erg s^{-1}) . However the observed flux of X-ray emission is only about 10^{30} erg s^{-1} . Hence, this hypothesis is also rejected.

- *Presence of circumstellar disk*: The system KH 15D has shown similar kind of eclipses that are associated to be of the circumstellar disk explained in Herbst et al (2010)[28]. Since the eclipse period was 16 days of the total orbital period of 48 days (the ratio of the eclipse period being one third of the orbital period), it was proved that the eclipse was caused due to circumstellar disk around the primary star. Similarly, a star named V718 Persei, also exhibits an prolonged eclipse of 1 year of its orbital period of 4.7 years as explained in Grinin et al. 2008[29]. Since the eclipsing object occupies most of the orbital plane, it was satisfactorily proved that the eclipse was caused due to the circumstellar disk present around the star. However, for J1407, the period is suggested to be greater than 850 days. Hence an eclipse of only 54 days will not support the hypothesis of circumstellar disk causing the eclipse since the ration of eclipse duration to orbital period is very small.

- *Presence of circumplanetary disk around the secondary*: It can easily explain the asymmetric dip in the flux. Mamajek et al.(2012)[9] modelled basic ring structure as shown in the **Figure 3.4**. The inner ring has to be very thick(optical thickness, τ=3) to produce a deep eclipse around HJD 2454225 days. The tilt of the ring is considered to be responsible for the asymmetric eclipse pattern. Thus the presence of circumplanetary disk around the secondary explains the photometric light curve. Hence a detailed modelling of the ring system is explained in the later section.

Figure 3.4: A basic ring model to fit superWASP data[9]

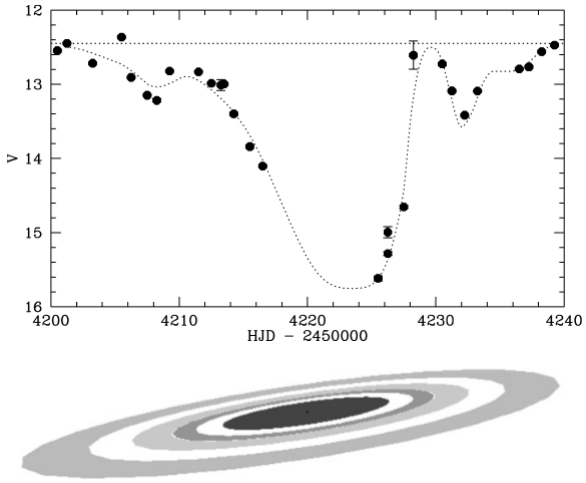

3.4. Modelling of the ring system

Research by Kenworthy and Mamajek (2014)[3] developed a detailed ring model that fits the transit data of J1407. The ring system is modelled by solving for the orientation of the ring system relative to the line of sight. Then from this information, the transmission of the rings is also solved to yield the complete model of the ring system.

Table 3.2: Disk model parameters[3]

Model	b (d)	t_b (d)	i_{disk} (deg)	ϕ_{disk} (deg)	$t_{\parallel}$ (deg)	v km s^{-1}
1	3.92	54225.46	70.0	166.1	54220.65	33.0

The **Figure 3.5 (a)** depicts the inclination of the ring plane with respect to the motion of the star. The motion of the star is approximated to be straight line and the secondary has a constant relative velocity with respect to the primary. The **Figure 3.5 (b)** represents the intensity of the light curve as the function of time. The **Figure 3.5 (c)** represents the variation of ring radius with respect to time. The three important epochs t_b, $t_\perp$ & $t_\parallel$ represent the epoch at which the star is closest to the secondary, ring tangent is normal to the relative motion of the star and ring tangent is parallel to the motion of the star respectively. The parameters which fit the data to the model are represented in the **Table 3.2**.

Figure 3.5: Geometry of the ring model[3]

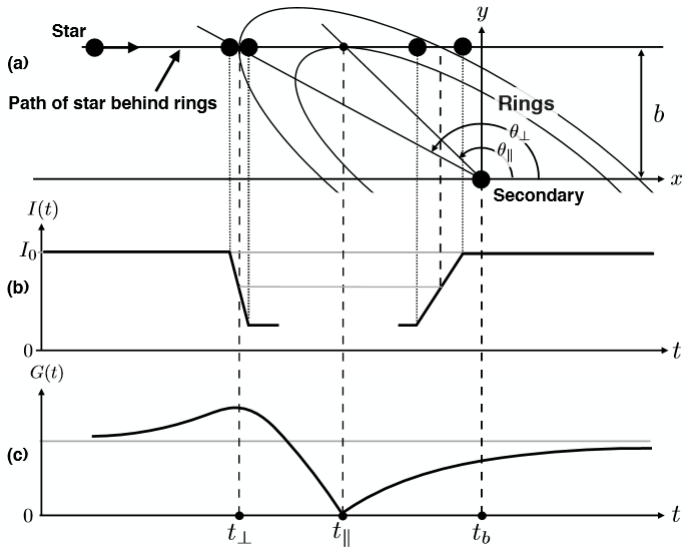

This research paper also suggests that the diameter of rings could possibly exceed the planet's Roche limit and hence there is a possibility of sculpting of the rings by the exomoons. The ring model is fit to the data by minimizing the value of χ^2 fit. From the ring model represented in the **Figure 3.6** it is evident that there are clear gaps and there is possibility of gravitational clearing by the exomoon or due to the Lindblad resonance caused due to the presence of other satellite in a longer orbit around the secondary. In the above entioned figure the green line through the rings represent the path of the star J1407. Higher intensities shown in the figure represent higher transmission by the particular region of the ring.

Figure 3.6: Ring model fit to the data[3]

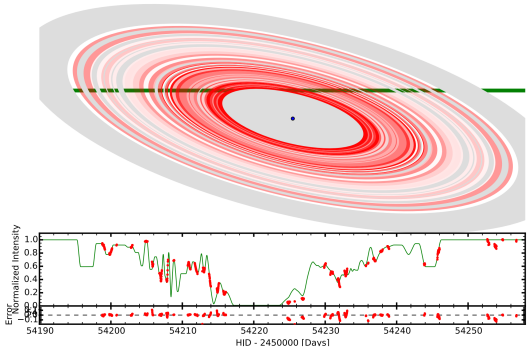

Research by Rieder and Kenworthy (2016) **[10]** strongly suggests that the ring system of the secondary should be retrograde. Using simulation model they have proved that the retrograde model could survive for a minimum of 10^4 orbits around the primary for a assumed period of 11 year and a maximum mass of $100M_{Jup}$.

Figure 3.7: Simulation of prograde and retrograde models[10]

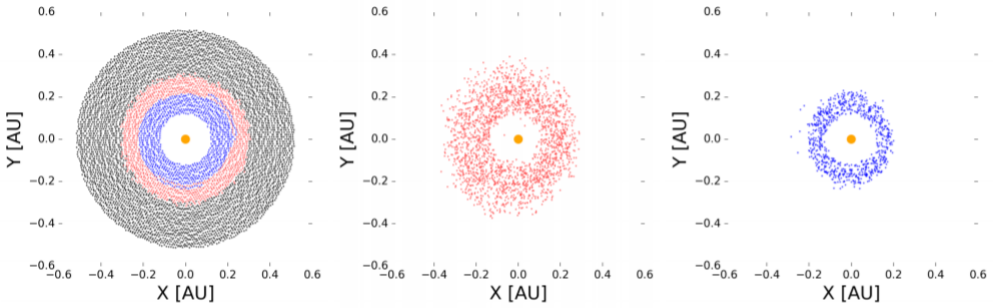

Figure 3.8: Eclipse duration for different models[10]

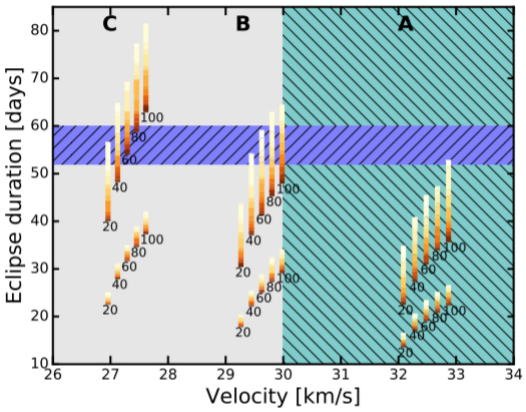

The research paper used three models namely A,B and C representing eccentric orbits with eccentricity values of 0.70, 0.65 and 0.60 respectively. **Figure 3.7** describes the evolution of particles

in the ring system after 0.1 million years.The left figure represent the initial configuration of particles. The middle case represents the retrograde and the right figure represent the prograde cases respectively for the model B with the assumption of mass of secondary to be that of 80 Jupiter masses. In prograde case, all particles greater than 0.45 $\pm$ 0.04 time the radius of hill sphere were lost due to the perturbation of the star at the periapsis, whereas in retrograde model particles are lost only for the radii greater than 0.64 $\pm$ 0.04 times the radius of the hill sphere. **Figure 3.8** represent the eclipse duration that each model are capable of producing. Upper models represent the retrograde case and lower models represent the prograde case. The color bar indicates the age of the ring system. Lightest color depicts the ring after 3000 years whereas the darkest of its tone depicts the age longer than 0.1 million years. It is very clear from the figure that only retrograde models are capable of producing an eclipse lasting a duration of 56 $\pm$ 4 days as seen with the photometric data. The eclipse duration for the prograde models are limited to a maximum of 40 days whose orbital velocity at periastron is less than the observed transverse velocity. Retrograde models show an eclipse of maximum of 80 days. Thus their research also emphasizes that younger retrograde ring models with lower eccentricites are capable of producing the required eclipse of 56 days as depicted by the observations.

3.5. Orbital Constraints

Research by Mamajek et al.(2010)[9] has ruled out orbital periods less than 850 days since the transverse velocity of this particular orbit will be less than 22 kms^{-1}. They have also rejected more than half of the orbital periods between 850 days and 2330 days. Research by van Werkhoven et al.(2014)[16] analysed the slopes obtained from the light curve during the eclipse of 2007 and have also ruled out the orbital periods less than 850 days. They have concluded in their research paper that even elliptical orbits could not explain the largest slopes seen during the eclipse of 2007. Hence,they have also propose the possibility of clumps or bars in the ring system, whose velocity will add vectorially to that of the transverse velocity of the secondary. In this scenario, the higher orbital periods with circular velocity will also satisfy the observed velocity gradient.

Detailed constraint models were presented in Kenworthy et al(2014)[11]. This research paper produced constraints using combination of photometry, transit and direct imaging data.

3.5.1. Direct Imaging

Sparse Aperture Masking(SAM) at the Very Large Telescope(VLT)[30] and Keck telescopes at W.M.Keck Observatory[31] were utilised to yield direct imaging constraints. J1407 was observed on 4^{th} April 2012 (Universal Time(UT)) with keck telescopes and also on 27^{th} March 2013 (UT) with the VLT. Both have resulted in a null detection with a 6σ limit with the keck and a 3σ limit with the VLT.

Direct Imaging Constraints

Since it was a null detection in both of the epochs, the angular separation of the secondary with respect to the primary for different orbital period is calculated. In the **Figure 3.10 (a)** the dashed and dotted lines represent the angular separation from keck and VLT data. BT-SETTL models from Allard et al.(2010)[32] were used to convert the sensitivity limits from the Keck and VLT data into upper mass limits of the secondary that are plotted as function of orbital period as shown in the **Figure 3.10 (b)**.

3.5.2. Photometry

The transit data were obtained from superWASP and ASAS. For the period of 9 years, no eclipse(except 2007) of J1407 were observed by these telescopes. New data for the 2012-2014 period was taken from Panchromatic Robotic Optical Monitoring and Polarimetry Telescopes (PROMPT)[33] and Remote Observatory Atacama Desert(ROAD)[34] which also showed no signs of any deep eclipses. However, data from ROAD and PROMPT has helped to rule out large orbital period between 4 and 7 years. PROMPT observations were taken with the help of V band and I band filters whereas ROAD used only V band filter.

Photometry Constraints

The grey vertical bars in the **Figure 3.10 (a) and (b)** represent the orbital periods that were ruled out transit data.

3.5.3. Radial Velocity

High resolution spectral images were obtained using the Magellan Inamori Kyocera Echelle(MIKE)[35] at the Magellan observatory on 2^{nd} February 2013 (UT). The wavelength range used was between λ = 3350-9500 Å with a spectral resolution R= 35000.

Another epoch was observed with CORALIE spectrograph[36] mounted at ESO's La Silla Observatory in Chile on 30^{th} May 2013 (UT) with a resolution R=60000.The RV data obtained from MIKE and CORALIE are represented in the **Figure 3.9**, where open circles represent the data obtained from MIKE and the closed circles represent the data obtained from CORALIE. It is important to note that the data from CORALIE are binned.

RV constraints

Radial Velocity model is constructed for orbits with $90°$(edge on) inclination. χ^2 fit is calculated for the model in comparison with the data which is shown in the **Figure 3.10 (c)** with the inclusion of 2σ, 3σ and 4σ limits.

Figure 3.9: RV data of J1407[11]

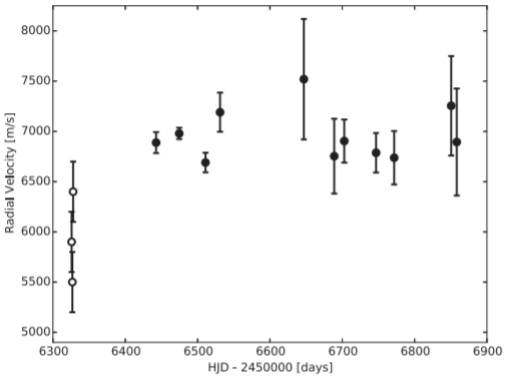

3.5.4. ξ constraint

Circular orbits

The value **Figure 3.10 (c)** represents the value of ξ expressed as the function of mass and period. The value of ξ equal to unity implies the extreme case where the entire hill sphere of the secondary is filled by the ring system. The research paper also suggested that the cases of $\xi > 0.4$ are highly improbable due to the results of research from Martin and Lubow et al. (2011)[37] which proposed the tidal truncation limit and also limits based on hydrodynamic simulations proposed by Quillen and Trilling et al. (1998)[38] suggested ξ limit to be that of 0.4 .

The values of ξ greater than unity are ruled out because the ring system would be unstable at those ranges. Thus a typical limit of $0.1<\xi<0.3$ are considered as suggested by the other research papers listed above.

Elliptical orbits

For orbits of high eccentricity, the hill sphere is not constant and its dynamics dependent on orbital position of the secondary. Hence the research by kenworthy et al.(2014) calculated the mean separation for the orbit os secondary having a particular value of eccentricity. The results of the ξ limit on the elliptical orbits are given in the **Figure 3.11 (d)**. The values of ξ constraints remain the same for elliptical orbit as discussed above.

3.5.5. Eccentricity Limit

The minimum eccentricity limit for the secondary can be calculated with the help of the transverse velocity(32 kms^{-1}) of the secondary observed during the eclipse. Only one particular value of eccentricity can satisfy the transverse velocity limit. It is calculated assuming that the orbit of secondary is edge on and the periastron is pointing towards the earth (ω=270 Ω=90). It is shown in the **Figure 3.11 (a)**.

Figure 3.10: period and mass limits for circular orbit of J1407b[11]

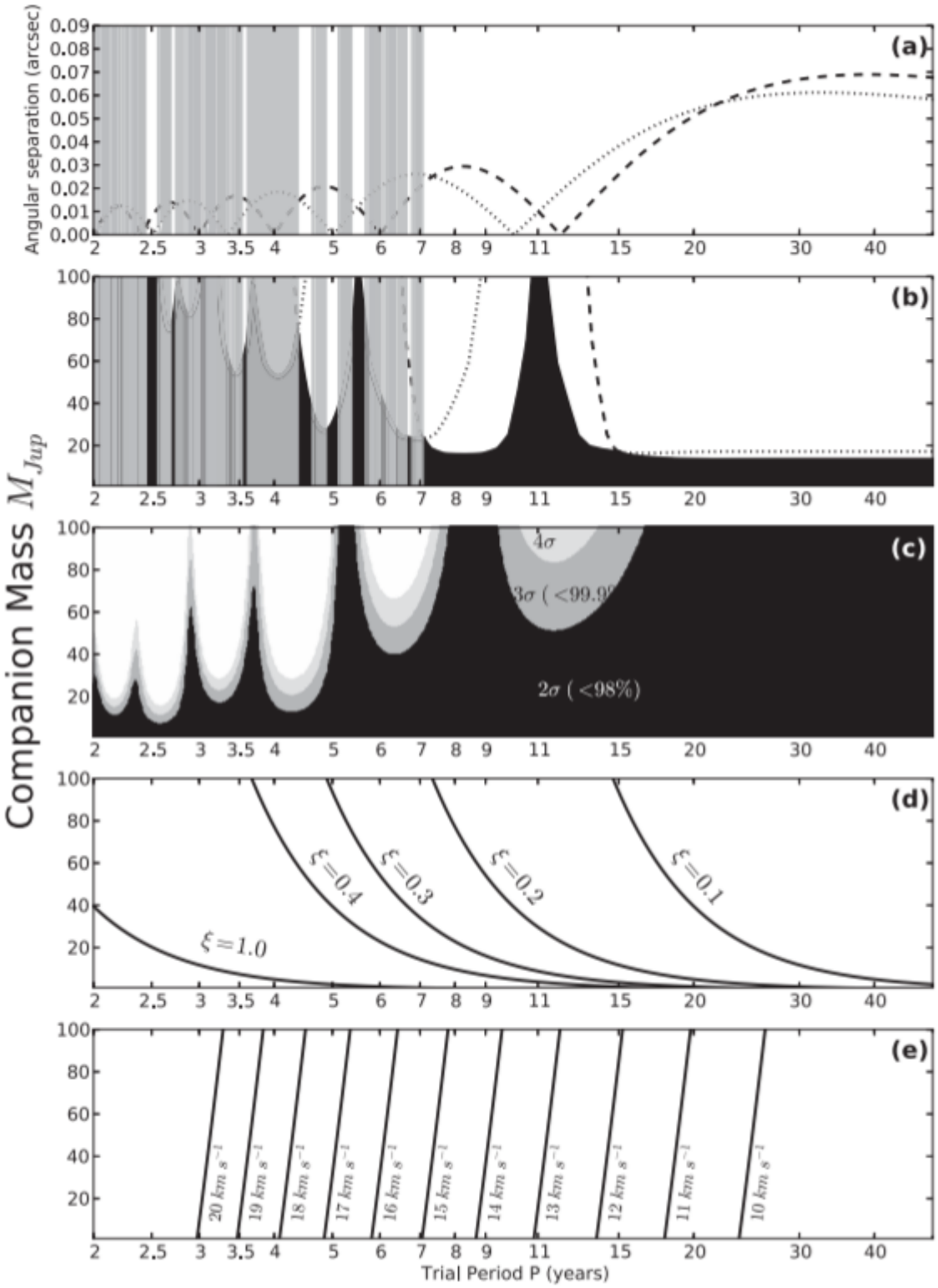

Figure 3.11: period and mass limits for elliptical orbit of J1407b[11]

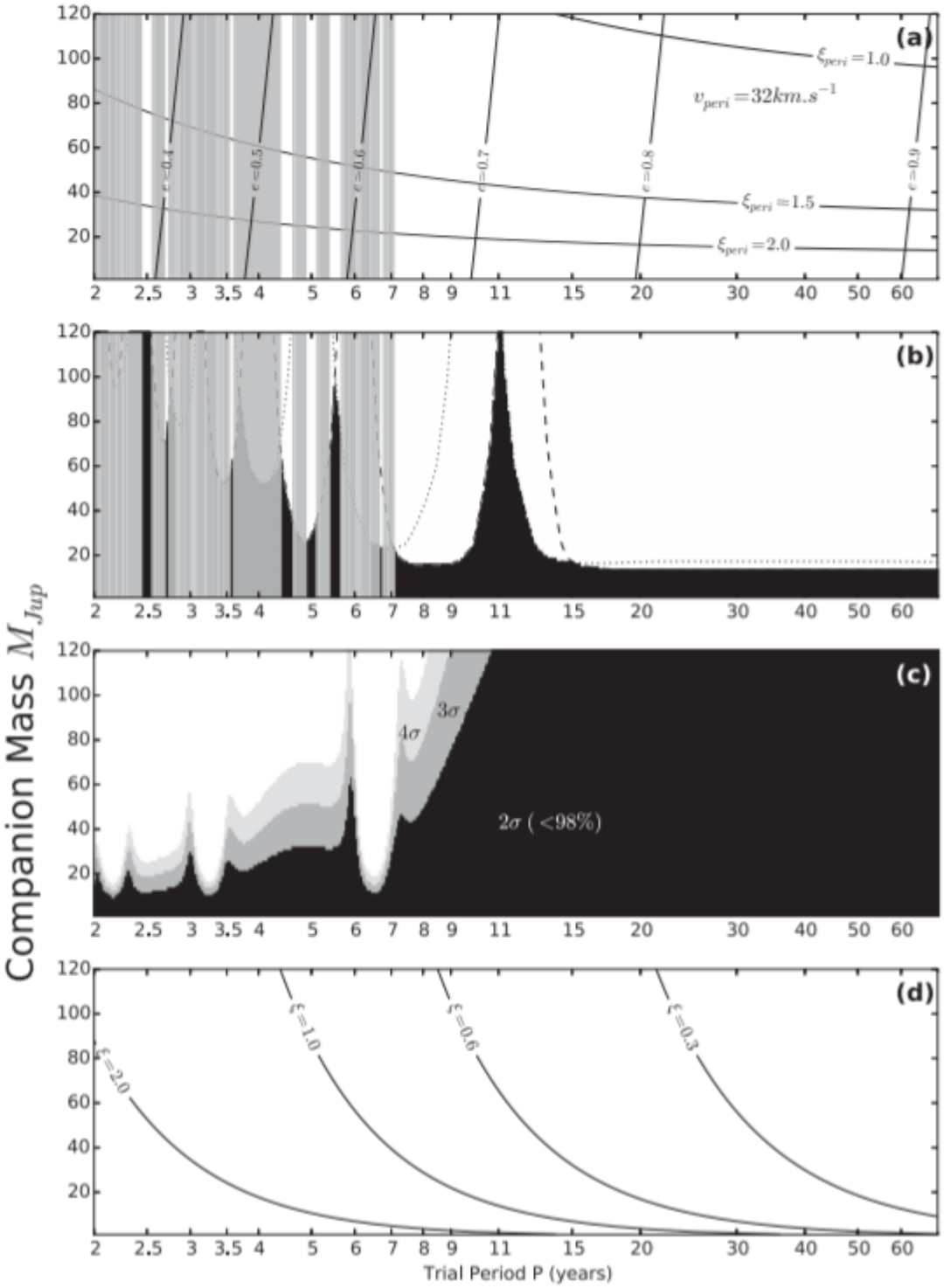

Figure 3.12: Combined period and mass limits for circular orbit of J1407b[11]

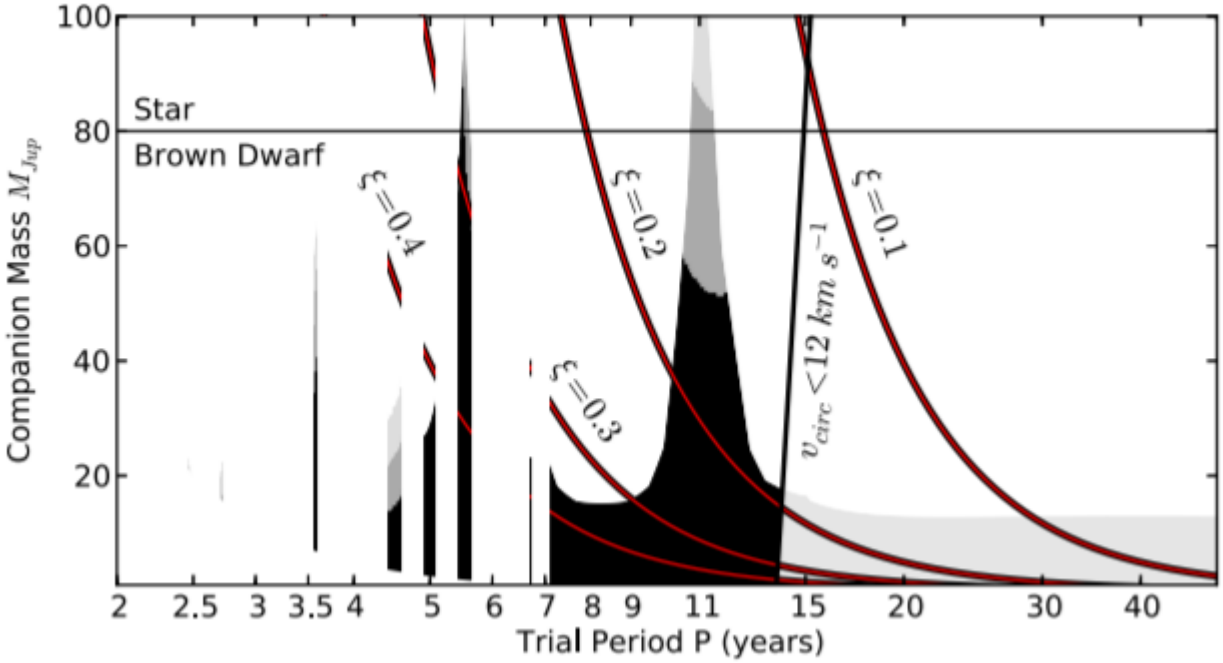

3.5.6. Mass and Period Limits

Circular orbit

Combination of results from **Figure 3.10** has been described as single figure in **Figure 3.12**. Direct Imaging does not provide any constraint for the orbital periods of 10 to 13 years. Radial Velocity does not provide any constraints for the orbital periods between 7.5 years and 10 years. From the figure the research paper concludes that the case of circular orbit is highly unlikely since the velocity does not match with the observed transverse velocity during the eclipse. Thus this scenario is only possible if the ring system is made up of large clumps of materials and the velocity of the clump material adds up to the transverse velocity of the secondary. In that proposed scenario, the orbital periods between 7 and 14 years prove to be the satisfactory solution.

Elliptical orbit

Combination of results from **Figure 3.11** has been described as single figure in **Figure 3.13**. radial velocity does not provide any constraint for the period grater than 11 years. However, Direct Imaging constraints the period greater than 11.5 years to a good extent and hence from the **Figure 3.13** we can see only an unconstrained limit between 9.5 and 12 years due to open constraints on mass from direct imaging results. Thus the results can be interpreted as, if the secondary's mass is greater than 20 times the mass of Jupiter then it must have the orbital period between 9.5 and 12 years.

Figure 3.13: Combined period and mass limits for elliptical orbit of J1407b[11]

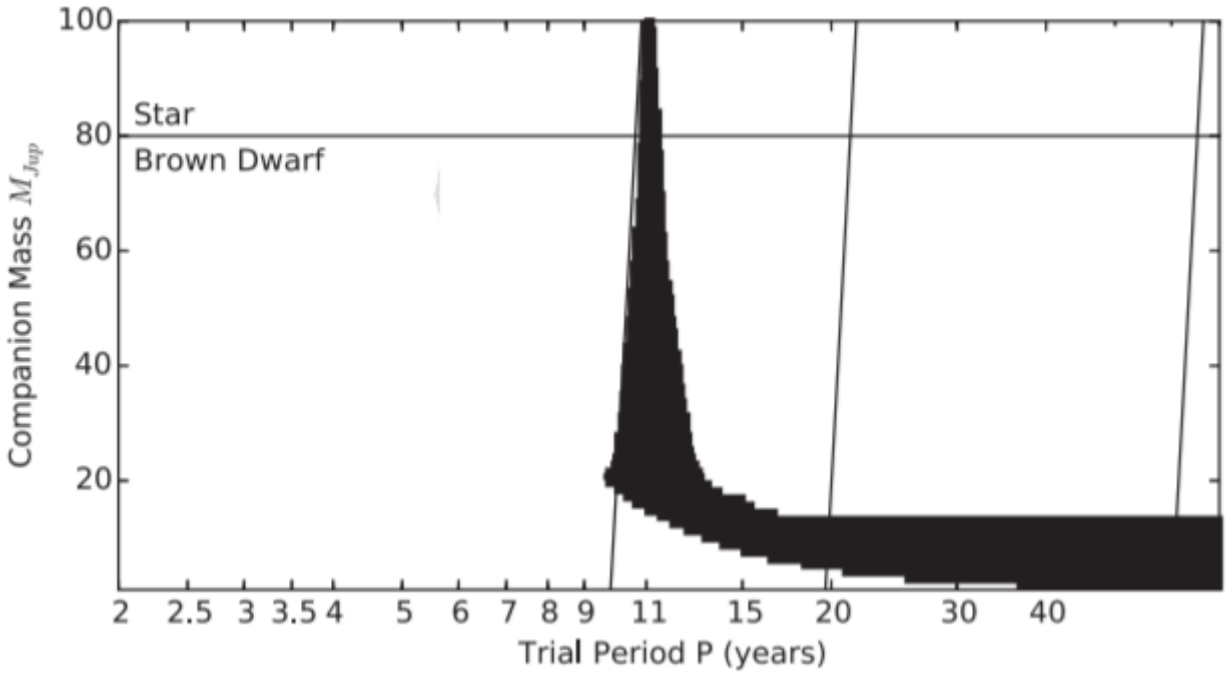

3.6. Conclusion

Research by Mamajek et al(2012)[9] gave insight into the Stellar mass($0.9M\odot$) and radii($0.99R\odot$) of J1407, which are almost similar to the sun but the star is way too young(16 Myr). Thus the star has high stellar activity which are evident from its eadial velocity data and the 3.2 days periodic rotation of star spots.

Light curve showed deep and long eclipses during April 2007, which has been confirmed with different sources of TRANSIT data. Further research by Kenworthy et al(2015)[3], proved that the eclipse might have caused by a complex ring system(other cases being ruled out by Mamajek et al.(2012)[9]) and modelled the ring system yielding important information regarding the geometry and orientation of the rings.

van Werkhoven et al(2014)[16] analysed the slopes in the transit data and gave insight into the maximum transverse velocity of the secondary.The research also suggested that the circular orbit is possible only when there are large clumps present in the disk of the secondary. Further research by Rieder and Kenworhty(2016)[10] proved that the rings must be retrograde in order to be stable for longer periods of time.

Kenworthy et al(2015) improved the understanding of the probable period and mass of the secondary by integrating the constraints from photometry, direct imaging, hill sphere and radial velocity

results and also reiterated that circular orbits are highly improbable.

4

Introduction to Orbital Parameters and Observation Techniques

In this chapter, several orbital parameters which are used in this report is explained along with the visual interpretation of the orbit of the secondary for various cases.Also the different techniques to detect an exoplanet are also included which will give an overall idea of how the data is measured and how it can be interpreted.

4.1. Definition of Orbital Parameters

True Orbit - Orbit of the secondary around its companion. It is also sometimes referred to as relative orbit.

Apparent Orbit - Due to the inclination of the orbit of the secondary companion in the plane of sky as seen from earth, its true orbit will be projected as apparent orbit in the plane of sky.

Line of nodes - It is defined as the line of intersection of the plane of apparent and relative orbit.

Ascending node - It is defined as a point on the line of nodes where the secondary companion moves away relative to the line of sight of the observer.

Semi major axis(a)- one half of the longest line segment that connects both the centre and the focus of the elliptical orbit. The centre is usually the centre of mass in case of a star and a massive secondary companion. Both the primary and secondary companion revolve around the centre of mass.

Period(P) - Period represents the time taken for the secondary to complete one full revolution around the centre of mass. From the Keplerian law, the time period(P) can be derived from the value of semi

major axis(a) with the formula

$$P = 2\pi \sqrt{\frac{a^3}{G(M+m)}} \tag{4.1}$$

where,

G represents the gravitational constant,

M represents the mass of the primary and

m represents the mass of the secondary.

Eccentricity(e) - It is the numerical eccentricity of the orbit of the secondary companion.

Time of periastron passage(T) - It represents the epoch(time), at which the secondary would be located exactly at its periastron.

Arbitrary time(t) - It usually represents the time at which the observations are recorded.Universal Time(UT), Modified Julian Date(MJD) , Barycentric Julian Date(BJD) are some of the commonly observed units.

Ω - It is defined as an angle between direction of north and the line of nodes of the apparent orbit measured through the east.

ω - It is defined as the angle between the ascending node and the periastron measured in the direction of secondary's rotation.

Orbital inclination(i) - It is defined as inclination of the true orbit with respect to the plane of the sky. It is always measured in counter clockwise direction (when viewed from earth).

4.2. Visualisation of orbital parameters

4.2.1. visualisation of inclination(i)

To explain the orbital parameter 'i', let us consider an arbitrary scenario of a star of 0.9 stellar masses having a secondary companion at an eccentricity value of 0.7 , having a periastron passage at 2007 and a period of 15.5 years. The value of ω and Ω are taken to be 270 and 90 degrees respectively. x-axis and y-axis in the **Figure 4.1** represents the separation of secondary(in arc seconds) in the plane of the sky when viewed from earth. The three plots in the **Figure 4.1** (from top to bottom) describes the inclination values of 0,50 and 70 degrees respectively. As the value of inclination increases, we can clearly see the magnitude of vertical separation is outdone by the magnitude of horizontal separation in the plane of the sky.

4.2.2. visualisation of Ω

Same arbitrary parameters as in the previous subsection are considered. In this case, let us keep the inclination to be fixed at 0 degrees(face-on) and the value of ω also to be fixed at 270 degrees. **Figure 4.2** (from top to bottom) represents the cases of 90,150 and 210 degrees respectively. It is very clear from the figure that the function of Ω is tilting the face of the orbit in the plane of the sky.

Figure 4.1: Plot describing inclination(i) of arbitrary companion in the plane of sky

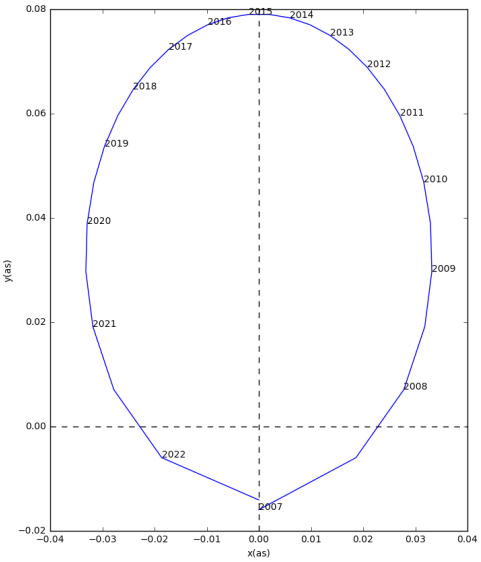

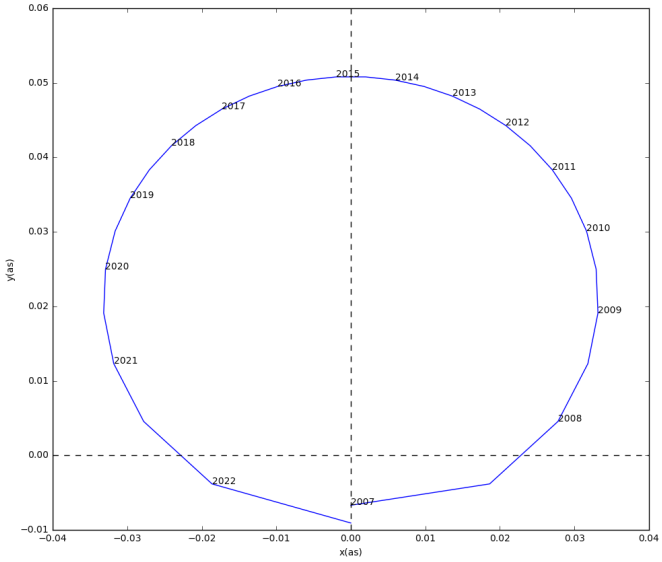

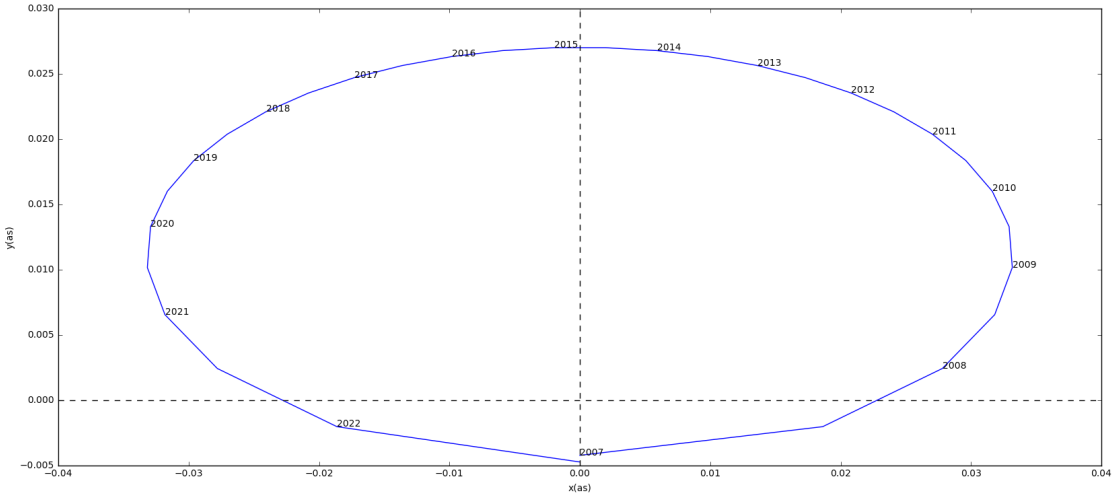

Figure 4.2: Plot describing Ω of arbitrary companion in the plane of sky

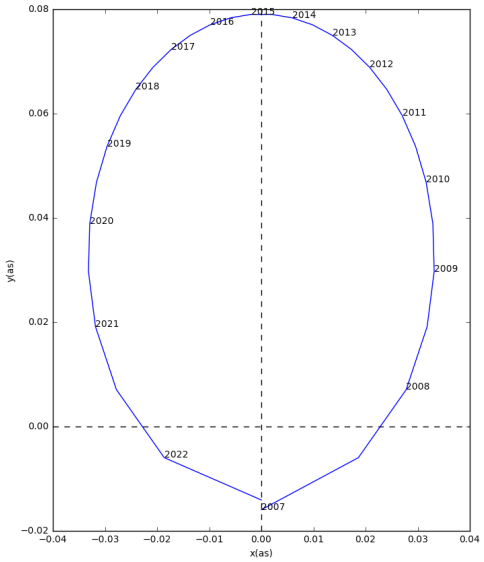

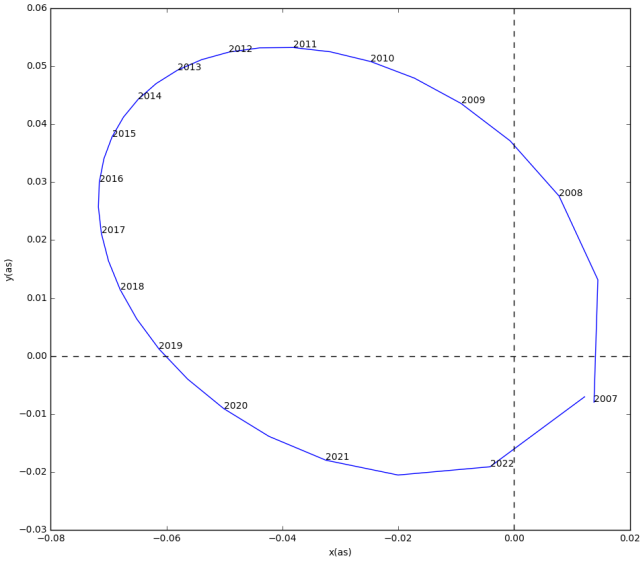

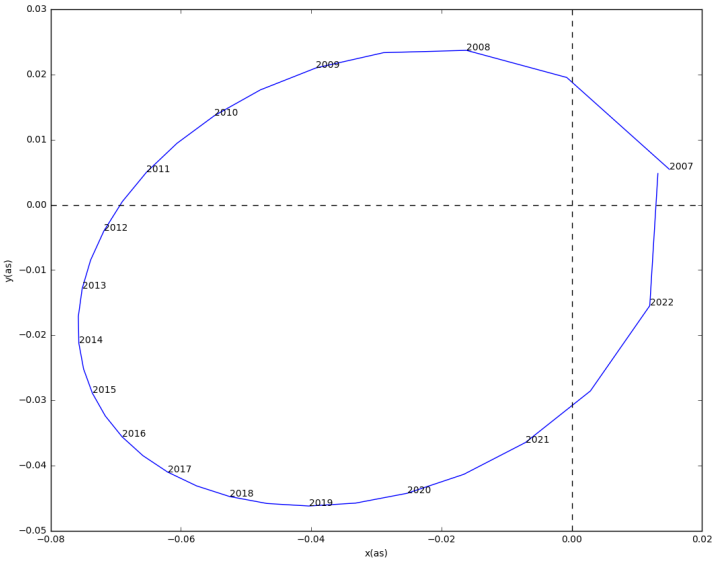

4.2.3. visualisation of ω

The **Figure 4.3** represents the arbitrary orbit of a planet to describe the value of ω. This orbit has an inclination of 0° (face-on) to yield a better understanding of the ω value. The top, centre and bottom represents the case of values of ω equal to 240, 270 and 300 degrees respectively. The position of the observer is in the direction of south i.e., for the value of ω=270 degree the periastron will be directly facing the observer. x- axis and y-axis are plotted in arc seconds taking into account the large distance of the star from the earth.The periastron and the apoapstron can be identified easily from the figure since they are plotted for a high eccentricity value of 0.7. The closest point from the centre of the ellipse is the periastron and the farthest point being the apoapstron. The periastron in the centre figure is about 2 arc seconds away from the star if viewed on a face-on orbit.

The **Figure 4.4** represents a clear case about the function of ω, where the top and bottom figures represents the case of ω equal to 270 and 90 degrees respectively. It is very clear from the figure that the function of ω is to change the position of periastron of the orbit of the secondary. For the value of ω=270 degrees, the periastron is considered to be closest to the observer in the plane of the sky for an edge on orbit.

It is important to note that ω deals with the true orbit whereas the value of Ω is associated with the apparent orbit, i.e., projection of true orbit in the plane of the sky. Thus changing the Ω changes only the orientation of the orbit in the sky and does not affect the results and the constraint. However changing the value of ω significantly affects the results. For example, if we change the value of ω from 270 to 90 degrees, the meaning of the result changes entirely, as we would be facing the apoapstron instead of periastron. This is the reason for the importance of ω in our research and thus the impact of ω will be concentrated and included in all our results and discussion.

Earlier researches by van Werkhoven et al(2014)[16] have suggested that the velocity observed during the transit is very high and is about 32 ±2 km s^{-1}. Hence, it is reasonable to assume that the secondary must have reached this high velocity at the periastron and the direction of periastron(ω=270°) must be facing the observer. But it is also possible for the secondary to have highly elliptical orbits(example: e=0.8,e=0.9) and values of ω less than or greater than 270 and still satisfy the velocity constraints at the periastron. Thus it is safer to assume the ω values between 250 and 300 degrees. Hence, hereafter, all the results of this research work will be displayed for different values of argument of periastron.

4.3. Development of Algorithm

It is very important to develop an algorithm to return the position and velocity of the secondary in x,y and z directions in the sky. Let us discuss how the algorithm has been developed from the basic orbital equations. the procedure is described below.

The mean angular motion(μ), described in **equation 4.2** is the magnitude of the angular velocity

Figure 4.3: Plot describing ω

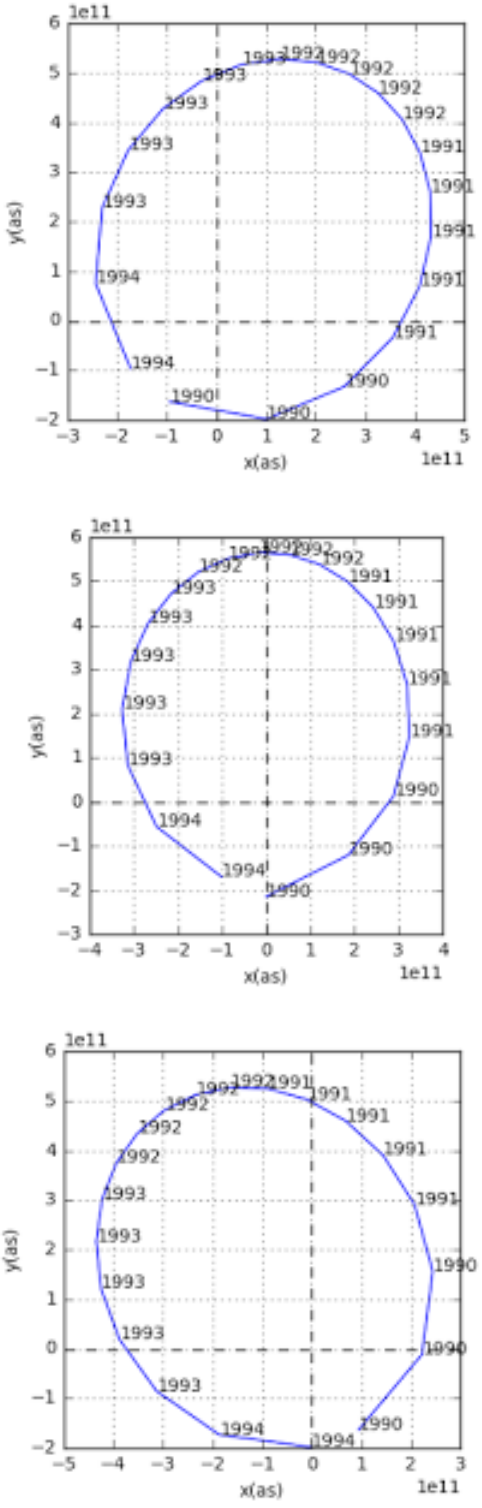

required by the revolving body to complete its one full revolution.

$$\mu = \frac{2\pi}{P} \tag{4.2}$$

Figure 4.4: Plot describing function of ω

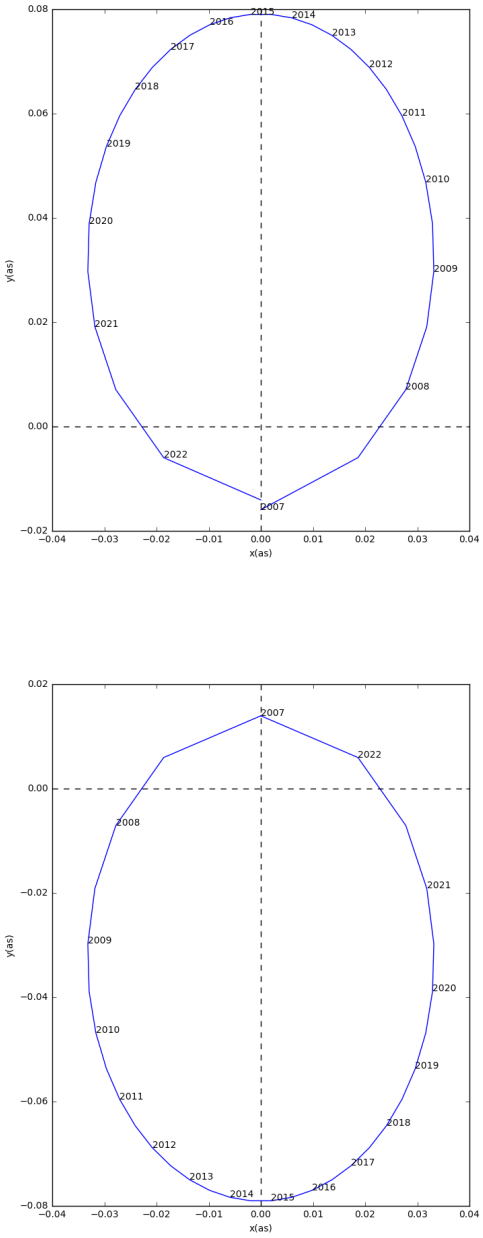

From the value of μ, the value of mean anomaly can be calculated, as mentioned in **equation 4.3**. The mean anomaly is used to measure the angular distance from the periastron at the arbitrary time(t).

$$M = \mu(t - T) \tag{4.3}$$

It is necessary to calculate the eccentric anomaly(E). For this an iterative technique is developed where an initial assumed(arbitrary) value of eccentric anomaly(E_0) is taken and it is iterated multiple times to

Figure 4.5: Position coordinates in the sky

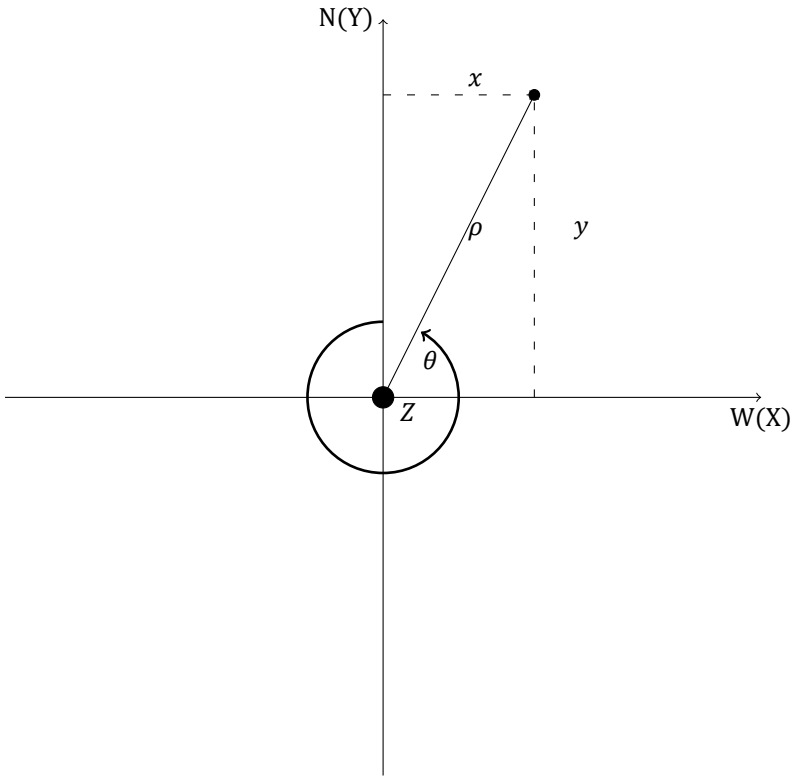

yield the final value of E as mentioned in the below **equation 4.4**.

$$E = E_0 + \frac{M - E_0 + e * sin(E_0)}{1 - e * cos(E_0)} \tag{4.4}$$

From the known values of eccentricity(e) and eccentric anomaly, the value of true anomaly(v) is obtained. True anomaly is defined as the angle between current position of the secondary in the orbit and the direction of the periastron and it is calculated from the known values as shown in the **equation 4.5**.

$$v = 2tan^{-1}\left(\sqrt{\frac{1+e}{1-e}}\right)tan^{-1}\left(\frac{E}{2}\right) \tag{4.5}$$

θ is defined as the position angle in the sky. **Figure ??** explains the coordinates and the meaning of angle θ. It is always measured counter clockwise from the north direction and it can be calculated from the known values as given in **equation 4.6**. 'r'represents the distance of the secondary from the focus of true elliptical orbit and can be calculated from the **equation 4.7**. ρ represents the projected separation of the secondary from its hose star in the plane of the sky and it is represented in the **equation 4.8**. ρ and θ represent the position of the secondary as cylindrical coordinates in the plane of the sky whereas the value of 'x', 'y' and 'z' represents the position of secondary in the plane of sky as Cartesian coordinates represented by the **4.9, 4.10 and 4.11** respectively.

$$\theta = \Omega + tan^{-1}\left(\frac{sin(\omega + v) * cos(i)}{cos(\omega + v)}\right) \tag{4.6}$$

$$r = a(1 - ecos(E)) \tag{4.7}$$

$$\rho = r\left(\frac{cos(v+\omega)}{cos(\theta-\Omega)}\right) \tag{4.8}$$

$$x = -\rho sin(\theta) \tag{4.9}$$

$$y = \rho cos(\theta) \tag{4.10}$$

$$z = rsin(i)sin(v+\omega) \tag{4.11}$$

The direction of z is in the direction of the observer. Similarly V_x, V_y and V_z represent the velocities in x,y and z directions respectively and they are described in the equations of **equations 4.12, 4.13 and 4.14** respectively. V_z is also described as the radial velocity. The radial velocity is positive when the star is moving away from us and it is negative when the star is moving towards the observer.

$$V_x = -\mu\left(\frac{a}{\sqrt{(1-e^2)}}\right)(esin(\omega) + sin(v+\omega)) \tag{4.12}$$

$$V_y = \mu\left(\frac{acos(i)}{\sqrt{(1-e^2)}}\right)(ecos(\omega) + cos(v+\omega)) \tag{4.13}$$

$$V_z = \mu\left(\frac{asin(i)}{\sqrt{(1-e^2)}}\right)(ecos(\omega) + cos(v+\omega)) \tag{4.14}$$

Thus the algorithm is capable of capable of computing the required positions(x,y,z) and velocities(V_x,V_y and V_z) in all the directions in the sky for the given orbital parameters of a,e,i,Ω,ω,t,T and P.

4.4. Introduction to Direct Imaging

Direct Imaging is the method of capturing the image of the exoplanets, which are planets orbiting the stars other than our sun. It is also classified as the only direct detection technique where the exoplanet is observed directly. High contrast ratios are required to detect the exoplanet directly since the stars are a billion times brighter than the planets themselves. Thus, coronographs are used to block the starlight in order to observe the exoplanet. Hence planets having large mass , possessing greater separation from its host star and younger planets which are hot and emitting lot of heat are easier targets to detect using this method. Planets which are having a face on orbits are easier to detect using this method since the face-on orbiting planets tend to have huge separation from its host star. Interestingly, planets that are not gravitationally bound to the host star can also be detected using this technique. For example, PSO J318.5 - 22[39] is a lonely young exoplanet of mass $6.5^{+1.3}_{-1.0}$ M_{Jup} associated with the β Pictoris moving group which was detected using direct imaging.

The first exoplanet to be detected by this method is HR 8799[12]. This image was taken using the Keck telescopes by using innovative techniques such as Angular Differential Imaging(ADI)[40, 41]

and Adaptive Optics(AO)[42] used by the Keck telescopes. In the **Figure 4.6** we could spot three planets HR 8799 b,c d which were found to be at a distance of 68,38 and 24 AU from their parent star respectively.

Figure 4.6: Direct Imaging of HR8799 system[12]

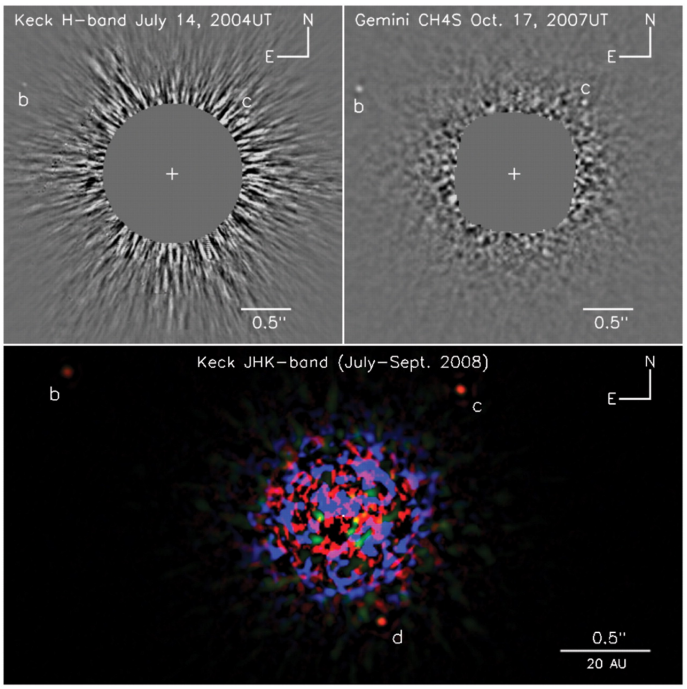

4.5. Introduction to Transit photometry

Photometry or Transit method is the most common method in finding exoplanets. It is the method by which the intensity of the electromagnetic radiation of the star is measured. Transit is a phenomenon in which the star's light is blocked by the body of the planet passing in front of it. **Figure 4.7** shows the integrated image at different epochs of time, taken by Solar Dynamics Observatory(NASA) [13]. When a planet passes in front of a star the observed flux of the star reduces and the flux regains to original magnitude again as the planet passes moves out of the line of sight of the observer with the star. There are different ground based missions such as Wide Angle Search for Planets(WASP)[26], MEarth project[43] and space based missions such as Kepler & K2 missions[44] developed by NASA and CoRoT(Convection,Rotation and planetary Transits)[45] developed by ESA.

From the **Figure 4.8**, parameters of transit curve can be identified. Large circle present at the centre of X and Y axis represents the star and the filled dark circles represent the position of the planet at different epochs. Time duration of t_I to t_{IV} represents the total duration of the eclipse. The regions t_I to t_{II} and t_{III} to t_{IV} represent the ingress and egress of the planet respectively. δ represents the total dip in magnitude caused by the planet and this parameter determines the radius of the planet.

The value of impact parameter represents the vertical separation of centre of the secondary to the

Figure 4.7: Integrated image showing the path of Venus transit[13]

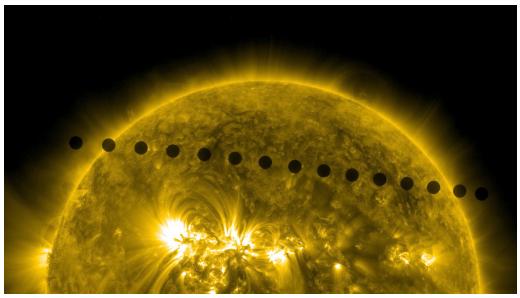

Figure 4.8: Illustration of a transit curve[14]

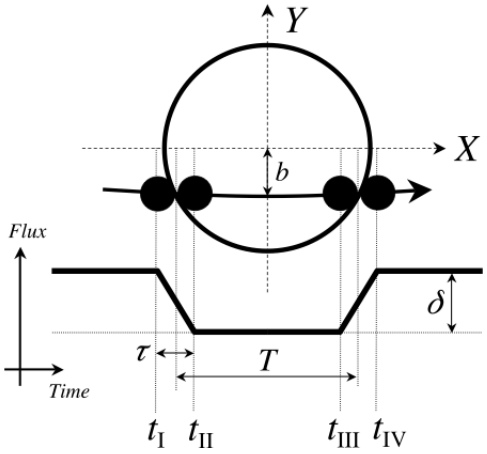

centre of the star measured at the point of closest alignment of star and the secondary in the plane of the sky. For example, if b=0, it implies that the centre of the star and the secondary are aligned with each other.

4.5.1. Importance of photometry

Transit method is the most important and simplest method when it comes to detection of exoplanets. Transit method has detected thousands of exoplanets.

The atmospheric modelling of the exoplanets can only be done with the transit data. the light passing through the atmospheres of the exoplanets are polarised and the study of this polarised light gives a good insight about the atmosphere of the exoplanets[46].

It is also important to note the limitations of the transit method. For example, the face on orbits(i=0°) does not produce any dip in the light curve since they do not pass in front of the star when viewed from earth. The transit data can also lead to False Positive(FPP) detection[47], which implies that the transit detections when followed by testing with the radial velocity detections indicate that the dip in the transit curve were caused by the eclipsing binaries or brown dwarfs rather than the planet.

4.6. Introduction to Radial Velocity(RV)

As mentioned in the **Chapter 4**, the change in the velocity of the star in the 'Z' direction is the radial velocity of the star. The radial velocity of the star is caused due to the secondary companion's gravitational tug on its star. Radial velocity is usually measured by the fundamental principle called as Doppler effect, with the help of a spectroscope. For example, from the below **equation 4.15**,

$$m_1 \, a_1 = m_2 \, a_2 \tag{4.15}$$

where,

m_1 represents mass of the star.

a_1 represents distance of the star of the centre of mass.

m_2 represents mass of the secondary.

a_2 represents distance of the secondary from the centre of mass.

it is clear that when distance of the secondary(a_2), from its centre of mass, becomes less, then it is compensated by the increase in the value of a_1. Thus the radial component also increases which is shown as a result in the spectrograph as the red shift(increase in distance of star from the observer, hence increase in wavelength of light) and blue shift(vice versa) will occur in the next phase of the secondary's orbit around its companion.

Figure 4.9 explains the radial velocity curve and the meaning of its components. The value of K is the semi amplitude of the radial velocity curve which can be calculated by the below **equation 4.16**

$$K = \frac{v_{r,max} - v_{r,min}}{2} \tag{4.16}$$

where,

$v_{r,max}$ represents the maximum magnitude of radial velocity

$v_{r,min}$ represents the minimum magnitude of radial velocity

From the known value of K, the minimum mass($m_2 sin(i)$) of the secondary companion can be calculation with the **equation 4.17**, with the assumption that $m_2 \ll m_1$. If the value of inclination is known, then the exact mass of secondary can be calculated.

$$K = \frac{2\pi G}{P}^{1/3} \frac{m_2 sin(i)}{(m1 + m2)^{1/3}} \frac{1}{(1 - e^2)^{1/2}} \tag{4.17}$$

where,

G is the universal gravitational constant.

The RV method has also its own set of drawbacks. If the star has lots of stellar activity, then the RV signal is filled with lot of noise. Sun spots also can change large magnitudes of change in the RV signal. The face on orbits(i=0°), the secondary moves in an orbit exactly in the plane of the sky and it inflicts the corresponding change in the velocity of its companion only in the transverse direction. Hence the change in the radial velocity of this kind of system will be equal to zero.

Figure 4.9: Plot describing the change in Radial Velocity of a star versus time [15]

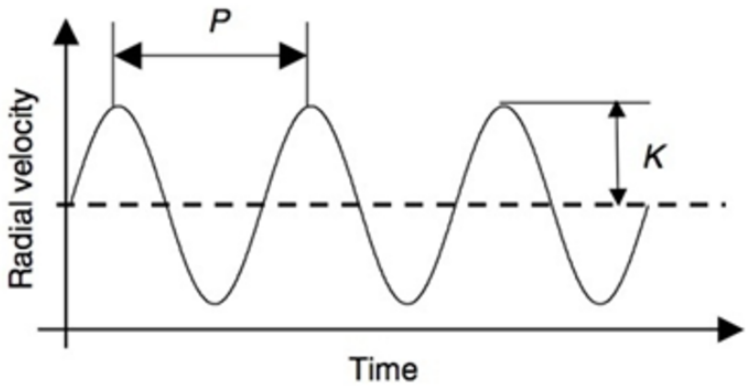

4.7. Conclusion

Thus from this chapter, it is clear how various types of data are obtained from different methods of exoplanet detection. It is also necessary to know the drawbacks of all the methods to know which method is well suitable to detect the exoplanet we are looking at. For example, as discussed earlier, if the exoplanet is having a longer orbital period and having lower values of inclination(close to zero degrees), then it is easier detect in direct imaging than with RV and transit method. J1407 is a young and active star with lots of noise and we know from earlier research papers by Mamajek et al.(2012)[9], that shorter orbital periods($<$ 850 days) are completely ruled out. Thus, out of the three techniques, Direct imaging will provide the most important constraint regarding the mass and period of the secondary J1407b compared to RV method, and transit method will provide the much needed velocity constraint and the value of impact parameter. In the upcoming chapters, the data obtained from J1407b are exclusively discussed and the constraints are mapped as the function of mass and period.

5

Inclination and Eccentricity Constraint

5.1. Introduction

Research by Kenworthy and Mamajek[3] modelled the ring system and have suggested that for the best fit scenario of the ring system, the value of impact parameter has to 3.92 days at MJD 54225.46 for a transverse velocity of 32 km s^{-1} of the secondary companion. Hence it is important to find the required inclination value that would match the condition that the secondary companion would be seen with the required impact parameter on MJD 54225.46. The value of eccentricity varies between 0 and 1 for elliptical orbits, having said earlier that the case of circular orbits have been ruled out. Thus it would be more visually easy to comprehend if we would be able to bring all the eccentricities into a single plot. Let us discuss in this chapter about how we achieve these two constraints.

5.2. Eccentricity Constraints

Observations from van Werkhoven et al([48]) has suggested that from the slopes of the transit plot observed, the transverse velocity of the secondary has been deducted to be equal to 32 ±2 km s^{-1}. Thus, assuming the secondary to be at periastron we can calculate the required value of eccentricity, for which the velocity of the secondary is equal to 32 km s^{-1}.

By rearranging the **equation 5.1** given below,

$$V_{periastron} = \frac{2}{P}\left(\frac{1+e}{1-e}\right)^{1/2} \tag{5.1}$$

and substituting the value of $V_{periastron}$ to be equal to 32 km s^{-1}, we obtain the critical value of eccentricity for each value of period P and mass of the secondary companion(m) , since the period value depends on the mass of the secondary as shown in the equation 4.1.

Figure 5.1: Eccentricity values satisfying the velocity constraint

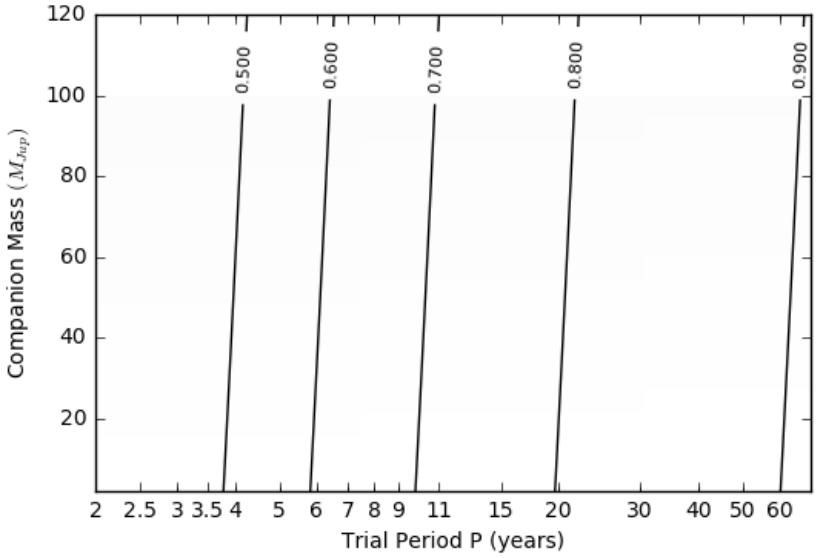

Figure 5.2: Critical eccentricity values from Kenworthy et al.(2015)[11]

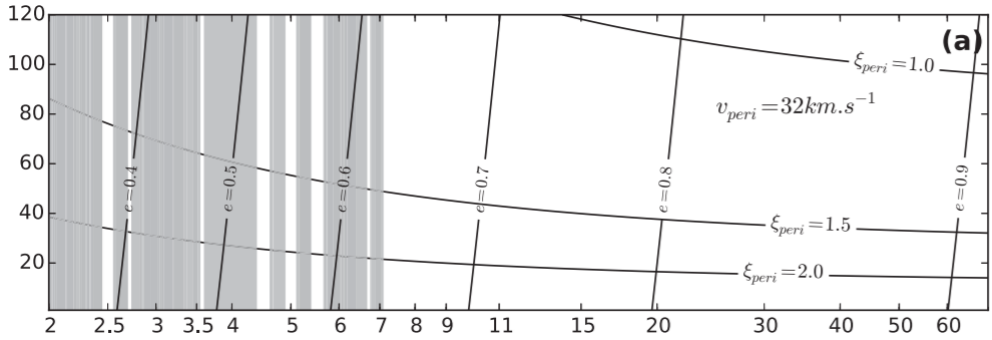

Figure 5.1 represents the minimum value of eccentricity which is required to satisfy the transverse velocity required at the periastron. The result has been generated by the algorithm developed and it is verified with the result from kenworthy et al.(2015)[11] as shown in the **Figure 5.2**. The black solid lines indicate the eccentricities required to produce the periastron velocity of 32 ±2 km s^{-1}. It is also clear from the figure that higher values of eccentricities are required for higher orbital periods in order to satisfy the transverse velocity requirement.

5.3. Inclination constraint

From the previous subsection it is clear that for each value of period(P) and mass(m) of the secondary companion there exists only one value of eccentricity full filling the transverse velocity constraint. Similarly there can also be only one value of the inclination which can satisfy the impact parameter(b) constraint. To achieve this we are going to use an optimization algorithm.

A grid search optimization algorithm is developed which provides a random set of input values of inclination between 50 and 90 degrees and the value of impact parameter is calculated for each value of inclination mentioned. After the first iteration, the inclination for which the difference between the required impact parameter and the calculated impact parameter is found. Then, the search space for the value of inclination is reduced to within 5 degrees and the process is repeated again till an accuracy of 0.001 AU for the impact parameter is reached.

Figure 5.3 represents the results obtained from the algorithm that shows critical value of inclination for different values of ω. From the figure it is evident that the value of inclination(i) that satisfies the impact parameter is different for different values of ω. It has already been suggested in the previous research studies on J1407b that it must have a value of ω equal or close to 270 degrees. Hence in the plots discussed in the report we have included the values of ω ranging from 250 to 300 degrees.

5.4. Conclusion

It is clear from the **Figure 5.3**, that the critical values of inclination that satisfies the impact parameter are almost in the range of 87 $\pm$0.5 $^\circ$. Thus the result also proves that the secondary companion cannot have the inclination of 90 degrees. The reason being that if the inclination will be 90 degrees, then the secondary would have been seen edge on and the entire body of the secondary would have also been observed along with its rings in the transit. However, it was not the case in the transit data and the model developed by Kenworthy and Mamajek(2014)[3]. In the research paper by Kenworthy et al.(2015)[11], the value of inclination was assumed to be 90 degrees. This result of the inclination is very critical and useful in representation of final results. Because, this result has incorporated, an additional constraint of inclination to the list of previous constraints in the earlier research studies.

Figure 5.3: Critical inclination values which satisfies the modelled value of impact parameter

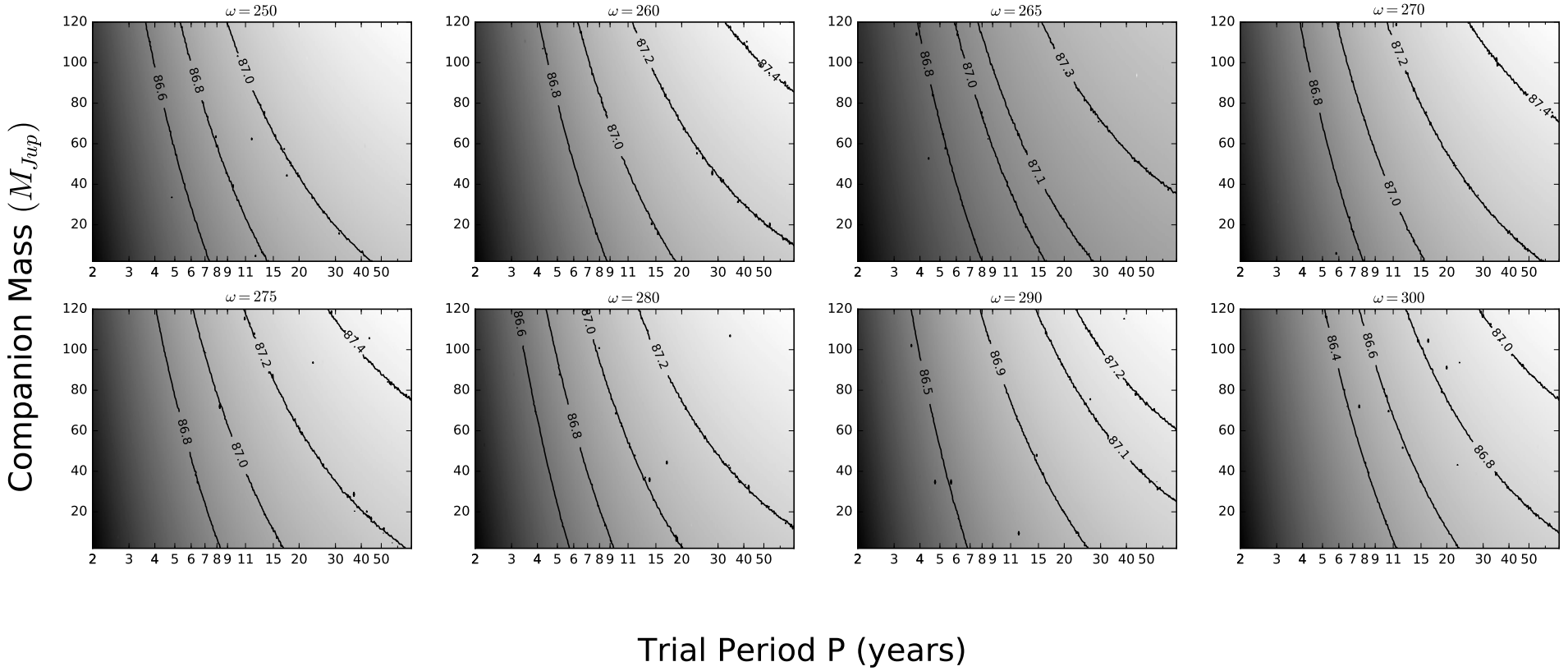

6

Direct Imaging

6.1. Observations of J1407

J1407 was observed on 4^{th} April 2012 (Universal Time(UT)) with the help of Keck-II Telescope and again on 27^{th} March 2013 with the help of Very Large Telescope(VLT). Both the epochs have resulted in null detection. Hence, from the respective epochs of direct imaging, the angular separation of the secondary for corresponding period and mass of the secondary are plotted.

In the **Figure 6.1 (a)** from Kenworthy et al.(2015), the dashed and dotted lines represent the angular separation in arc seconds for the respective direct imaging epochs observed by VLT and Keck respectively. They are converted into the function of upper mass limits with the help of BT-SETTL models developed from Allard et al.(2012) [32]. The algorithm uses the distance and age of the stellar system and calculates a sensitivity map in delta magnitudes for the respective position of the sky which in turn are converted into the upper mass limits as shown in the **Figure 6.1 (b)**. From the above mentioned figure it is very clear that mass constraint opens up for the region of orbital period of 11 years.

Hence, new observation was carried out on 16^{th} June 2016 , with the help of Keck-II telescope and it also resulted in null detection. But, applying the same procedure with the new data has resulted in new mass and period constraints. New algorithm to include the latest observation of direct imaging, was developed as a part of this research and the results are verified with Kenworthy et al.(2015) which are presented in **appendix 11.2**.

In the top plot of **Figure 6.2**, the angular separation of J1407b assuming a circular orbit has

Figure 6.1: Constraints for circular orbit of J1407b[11]

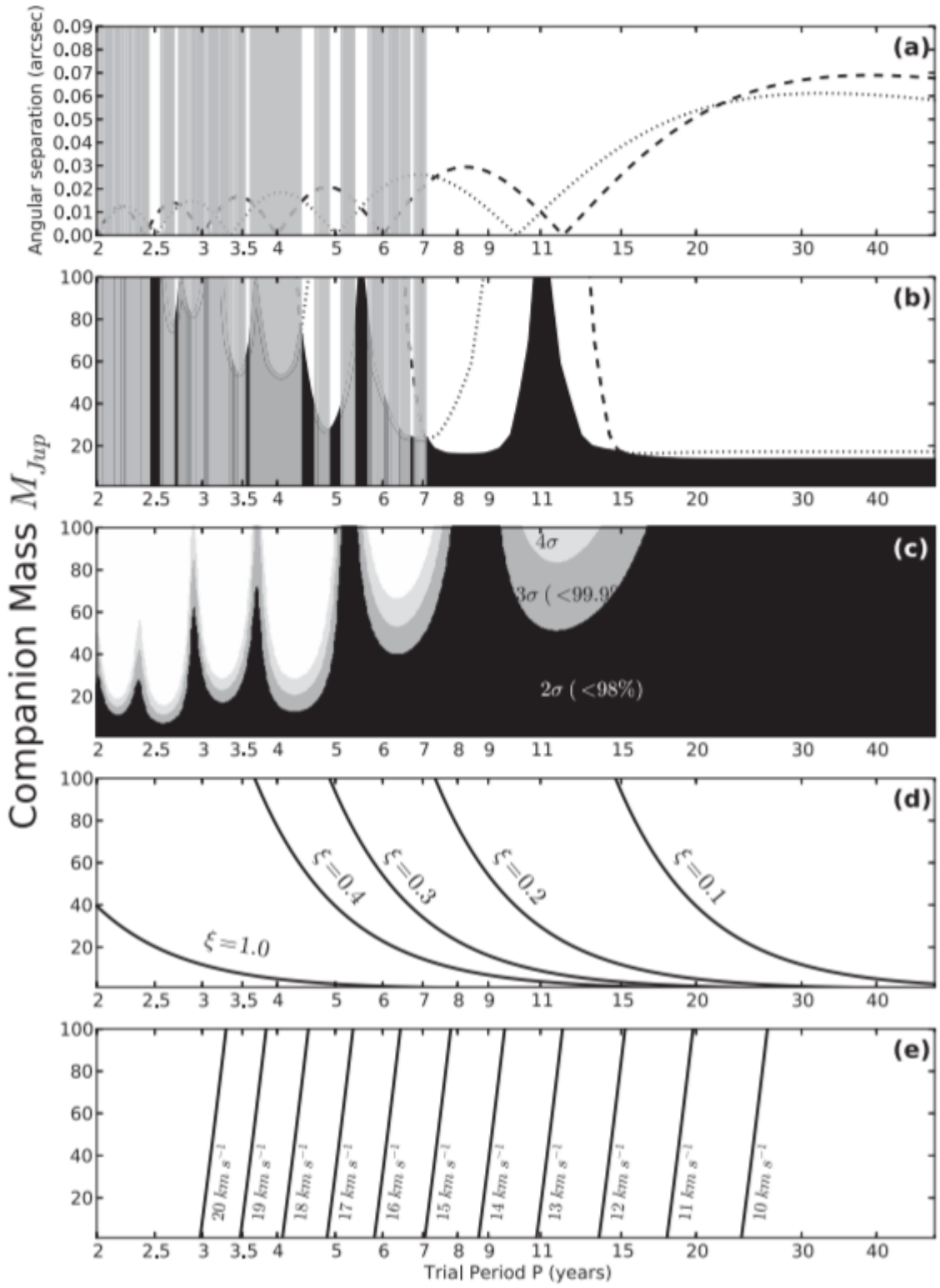

been plotted for three different epochs of direct imaging. In the bottom plot, the angular separation are converted into upper mass limits and we can clearly visualise the difference with **Figure 6.1** that

the mass constraint opening around P=11 years has been well constrained to about 45 Jupiter masses. Thus with the help of third epoch of direct imaging from Keck we have achieved a new mass constraint.

Figure 6.2: Direct imaging constraint of J1407b(circular orbit)

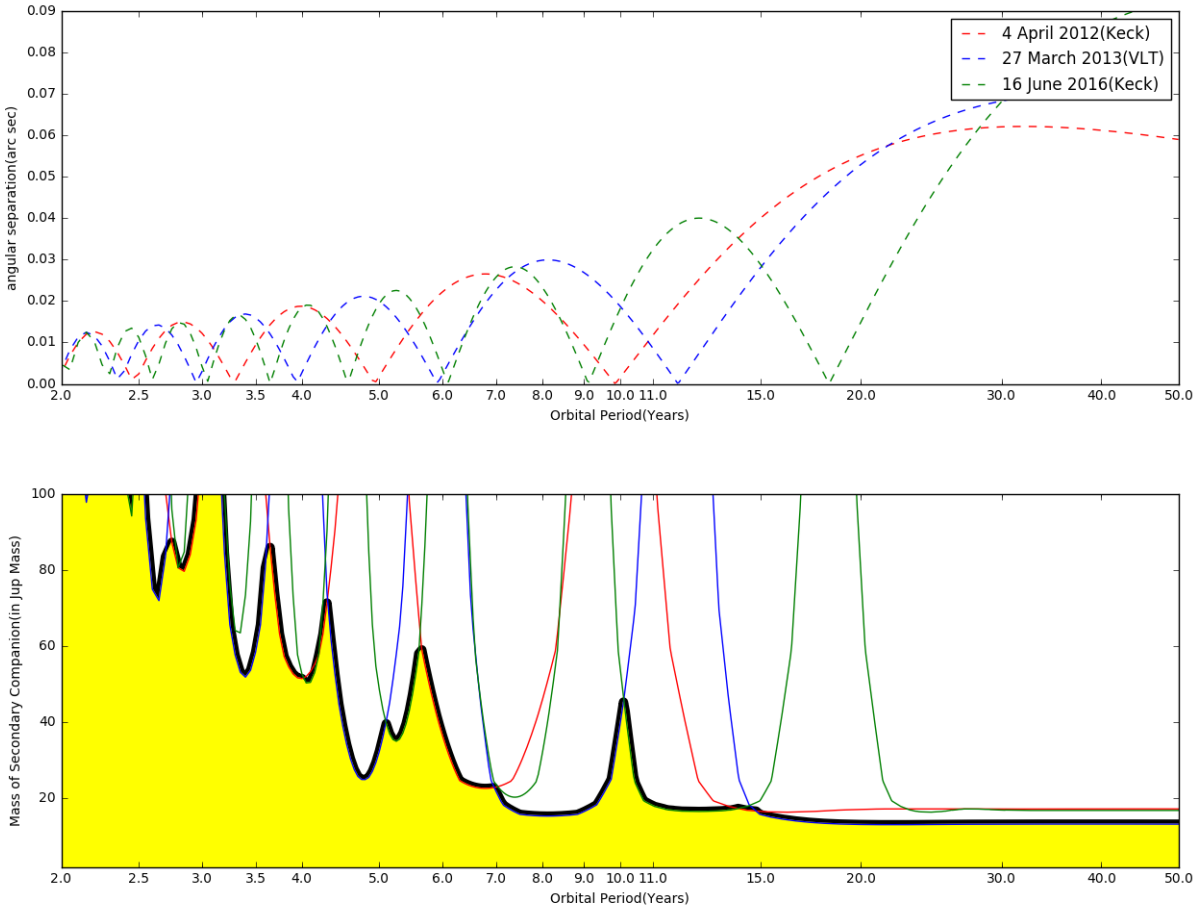

This can also be verified with the help of **Figure 6.3**, where the big yellow circle represents the blob obtained as the result of diffraction in the direct imaging telescope. The red dot in the circle is the actual size of the star J1407 (magnified 10 times for the sake of clarity). The radius of the central blob is given by the below equation 6.1

$$\theta = 70\frac{\lambda}{D}\ (degrees) \tag{6.1}$$

where,

λ represents the wavelength of light,

D represents the diameter of the mirror of direct imaging telescope.

The blue(visible), green and brown(invisible and hidden behind the central blob) represent the size of J1407 with the rings being present face-on. The radius of ring system is assumed to be 3.74

milli arc seconds. In the **Figure 6.1** it is clear that the constraints are open at the period of 11.2 years. From the **Figure 6.3** it is clear that both the epochs (April 2012 and March 2013) mentioned in the research paper are hidden behind the central blob and are thus, invisible. Since the June 2016 epoch from Keck is far outside the central blob, new results mentioned in **Figure 6.2** have a new mass constraint and the result implies at 11.2 year orbital period the secondary would have went unnoticed only if it is less than 20 Jupiter masses.

Figure 6.3: Position of Secondary Companion during various epochs of direct imaging

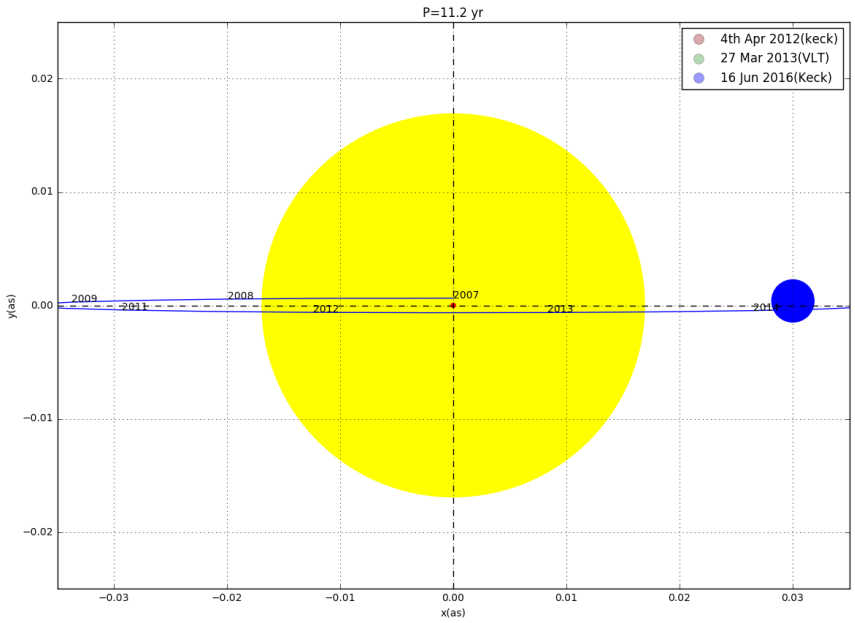

Applying the same technique and using the eccentricity constraint mentioned in the **Chapter 5**, we get new direct imaging constraints for elliptical orbits which are shown in the **Figure 6.4**. This figure explains the constraint for different values of ω and it is also important to note that each value of mass, period and omega has a unique value of inclination and eccentricity which satisfies the constraints mentioned in **Chapter 5**. In the figure , the green dotted, black dashed and the red dotted lines represent the direct imaging epochs of Keck(2016), Keck(2012) and VLT(2013) respectively. The black region represents the possible mass and period which the secondary can possibly have. The figure also implies that for higher the value of ω and with the increase in orbital period, the secondary can probably be a brown dwarf of up to 60 Jupiter masses and possibly have large eccentricity.

For the case of smaller values of $omega$, like $\omega = 250$, if 10 year orbital periods are ruled out by the transit photometry data, then the figure implies that the secondary cannot have very large mass(>20 M_J).

6.2. Conclusion

Thus direct imaging technique is the most useful technique when it comes to ruling out large orbital periods. The reason being , when the secondary is far way from its companion star(thus higher orbital periods), it is also far away from the glare of the star and thus it is easier to detect it. **Figure 5.8** also proves this as for all cases of $\omega < 280°$, larger orbital periods for secondary possessing the mass greater than that of 20 M_J is completely rejected. Even the greater peaks in the smaller orbital periods(< 10 yr) will be cancelled out if the transit data shows no signs of secondary companion in the fist 10 years of data, which will be discussed in the next chapter.

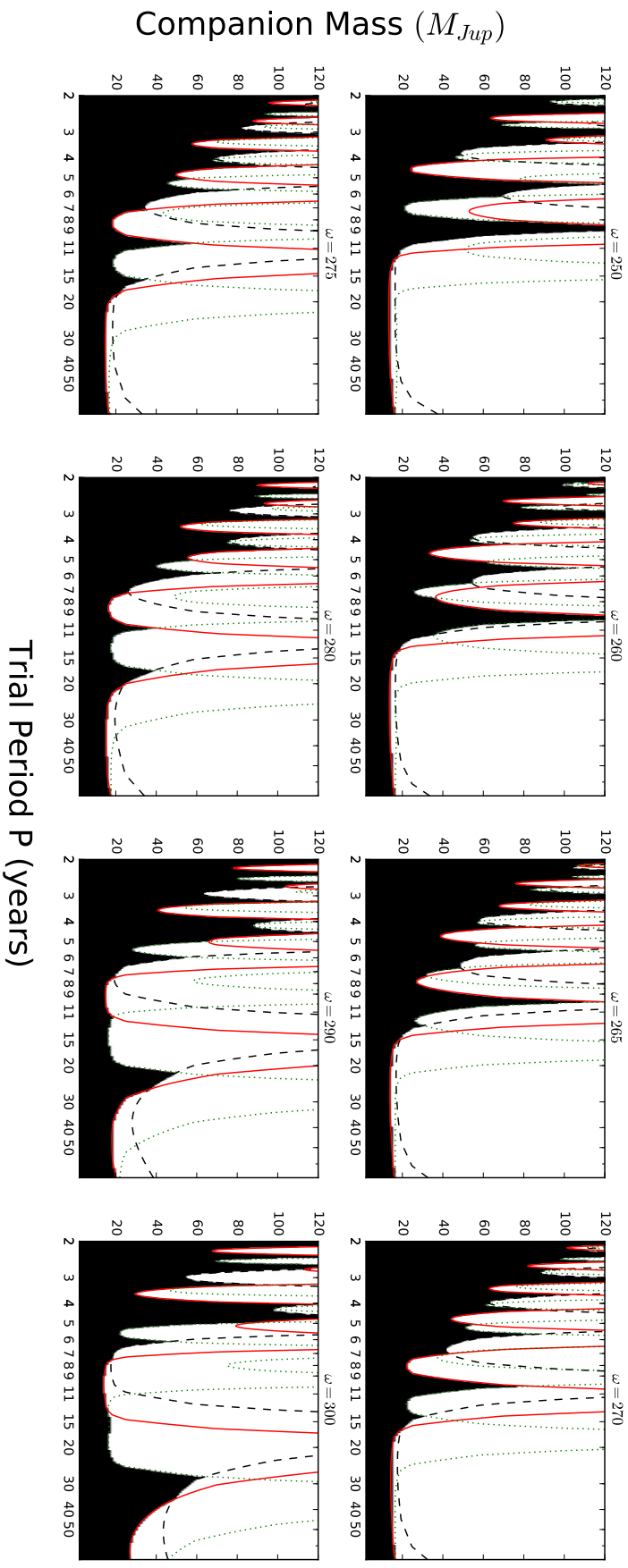

Figure 6.4: Direct Imaging constraints for elliptical orbits

7

Photometry

7.1. Photometry data of J1407

In the previous research papers by kenworthy et al[11], the transit data were incorporated for upto a period of 7 years. In our new results we have included transit results of up to 10 years from the data obtained from The All Sky Automated Survey(ASAS)[18].

An algorithm for period folding of transit data is developed. **Figure 7.2** represents the period folded results for 3.2 days of the new transit data. The sine curve fitting the data points strongly implies the presence of solar activity and sun spots with a rotation period of 3.2 days. This also proves the result from **Figure 7.1** and the new data results implies that the star spots are prominent even today. This also verifies our algorithm.

Moreover the transit data points are analysed and are folded consecutively for a period of 10 years in steps of one day interval. If there is at least one data point observed in the interval of 56 days(duration of eclipse), then the time period is ruled out which is shown in the **Figure 7.3**. The blue bar indicates the time period which are completely ruled out. It is clear from the figure that most of the region in the period interval of 10 years are blocked out except for some small intervals in 6 and 6.5 years.

It is important not to neglect the gaps where there are no transits seen. A very good example is the recently discovered PDS 110 system. It has an orbital period of about 808 days[17]. In the **Figure 7.4** the gray vertical dashed lines show the exact period when the eclipse has taken place. It is clear from the figure that the first three eclipses have been missed by the observers. Only in 2009 they were successful in capturing the eclipse data, which also showed an asymmetrical pattern implying the presence of giant ring system. Similarly the gaps in the period of 6 and 6.5 years of observations of

Figure 7.1: 3.2 days phase folded results from van Werkhoven et al.(2014)[16]

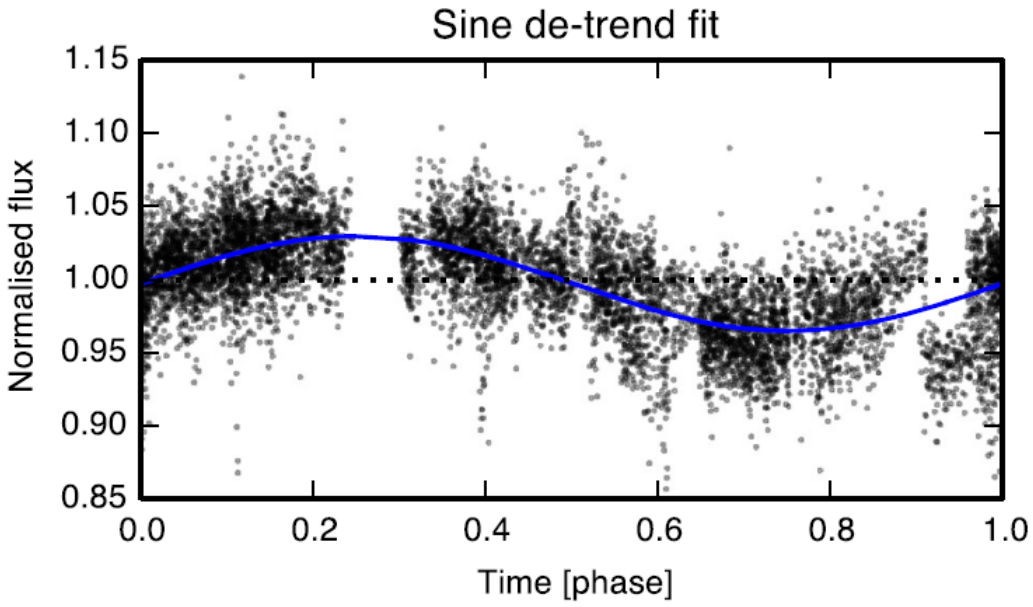

Figure 7.2: 3.2 day period folding result for transit data of J1407b

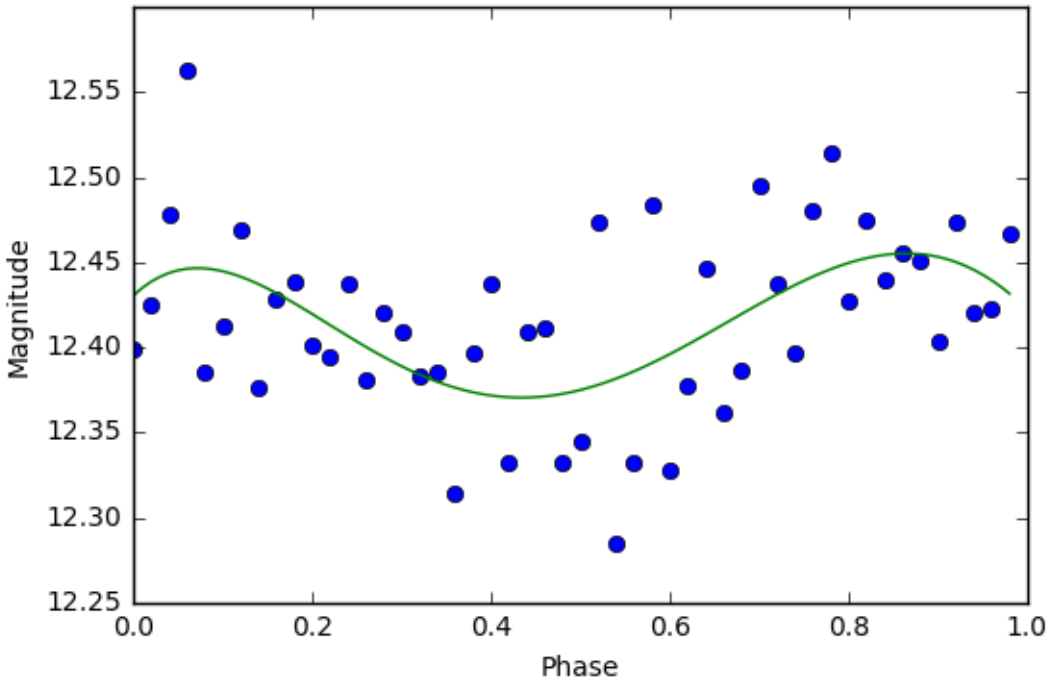

J1407 cannot be ignored. The data taken in the year 2019(12 years from the first eclipse in 2007) will help us to verify whether the secondary has a six year orbital period or not. The reason being 12 years is a multiple of 6 year orbital period. Since we have missed out in 2013, we can ignore the 6 year orbital period if the star does not show any signs of transit in 2019. Similarly the orbital period of 6.5 years can also be ignored in the case we get observations of 2020.

Figure 7.3: Photometry constraints of J1407b

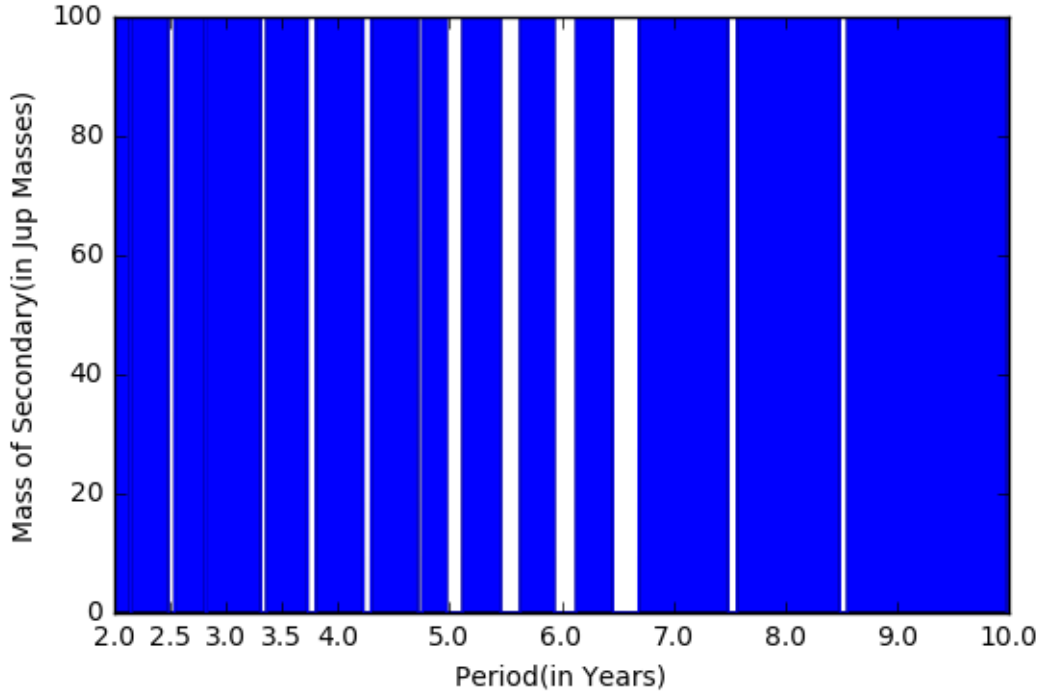

Figure 7.4: Photometry data of PDS 110[17]

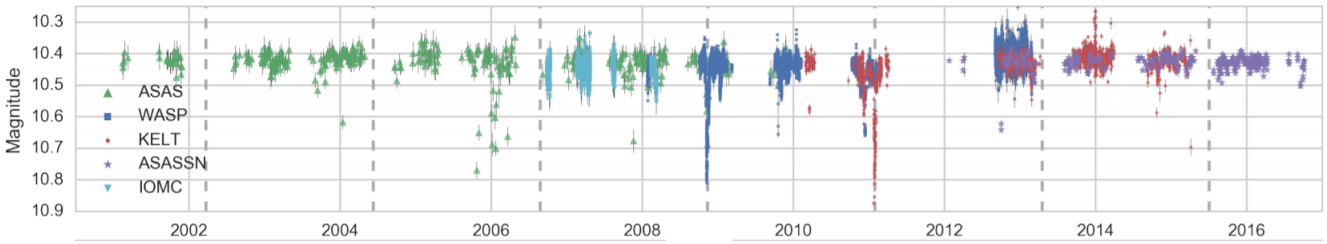

7.2. Conclusion

Transit observations of J1407 should show a greater than 2 mag deep dip as shown in **Figure 7.5**. However, for the past 7 years of observation the transit observations have never showed any dip greater than 2 magnitudes. **Figure 7.6** shows the transit data from 2012 to May 2017 taken by ASAS and it is clear from the figure that there are no greater than 2 magnitude deep eclipses(except for the period in which there are no data(gaps)). If the eccentricity of J1407b is very high, then there is a possibility that the hill sphere of the secondary may shrink at the periastron giving away the particles in the ring to the parent star. Thus the depth in magnitude may not be the same as we observed in 2007. Thus it is expected at least the secondary should exhibit a greater than 2 magnitude deep eclipse. Hence we can conclude that orbital periods for J1407b has been completely ruled out for the regions shown

in the **Figure 7.3**.

Figure 7.5: superWASP photometry light curve of J1407[9]

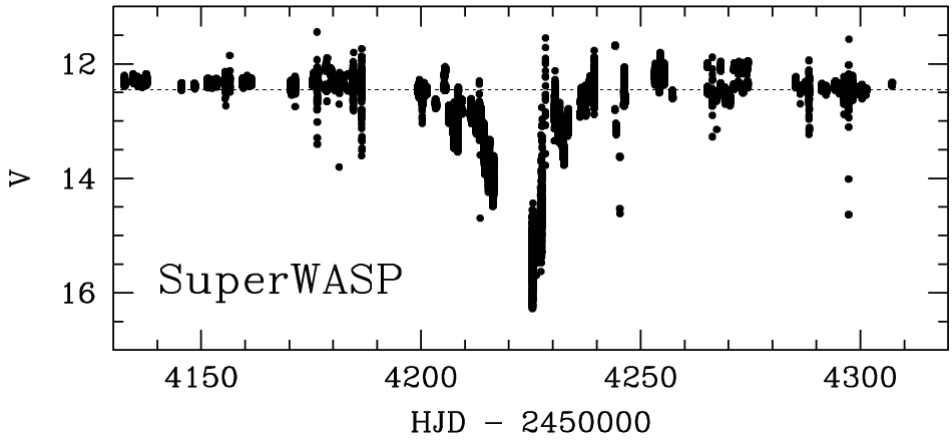

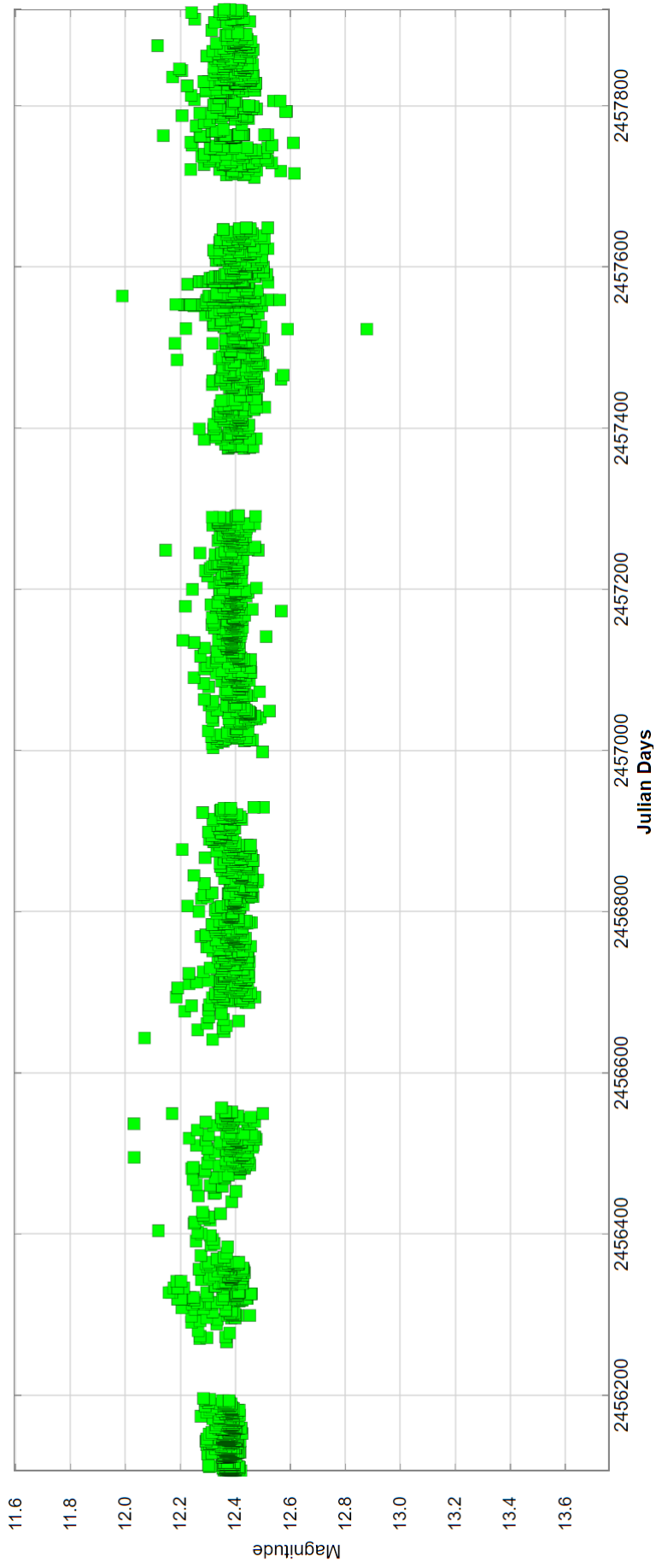

Figure 7.6: Transit light curve of J1407 for the past 5 years[18]

8

Radial Velocity

8.1. Radial Velocity data of J1407

Radial Velocity data are taken from fibre fed and thermal controlled CORALIE spectrograph mounted from Leonard Euler Telescope at La Silla Observatory(Chile) established by the European Space Agency(ESA). CORALIE planet search program has been active since June 1998 and has detected several exoplanets since its first discovery of Gliese 86b by Queloz et al[49].CORALIE was upgraded in the year 2007[50] to yield a improved resolution of about 60000 with an accuracy of about 6 m s^{-1}.

Details regarding the updated radial velocity data of J1407b are given in the **Figure 8.1** and are explained below.

Figure 8.1 (a) represents the updated RV data of J1407 plotted against time after the subtraction of its mean systemic velocity ,γ=6.91 ±0.04 km s^{-1}.**Figure 8.1 (b)** represents the CORALIE data measurements of Full Width at Half Maximum(FWHM) implying a very active star with lots of activity.**Figure 8.1 (c)** represents the span in the slope of the bisector of the RV data also implying a very active and young star. Stellar activity can be easily proven when there is anti-correlation between the RV data and slope of bisector. Thus, **Figure 8.1 (d)** represents RV data plotted against the slope of the bisector which shows strong anti correlation proving a prominent stellar activity during the course of the observation.

8.2. Constraints for Circular Orbit

Constraints from the radial velocity data can be obtained using a technique called as χ^2 fit.

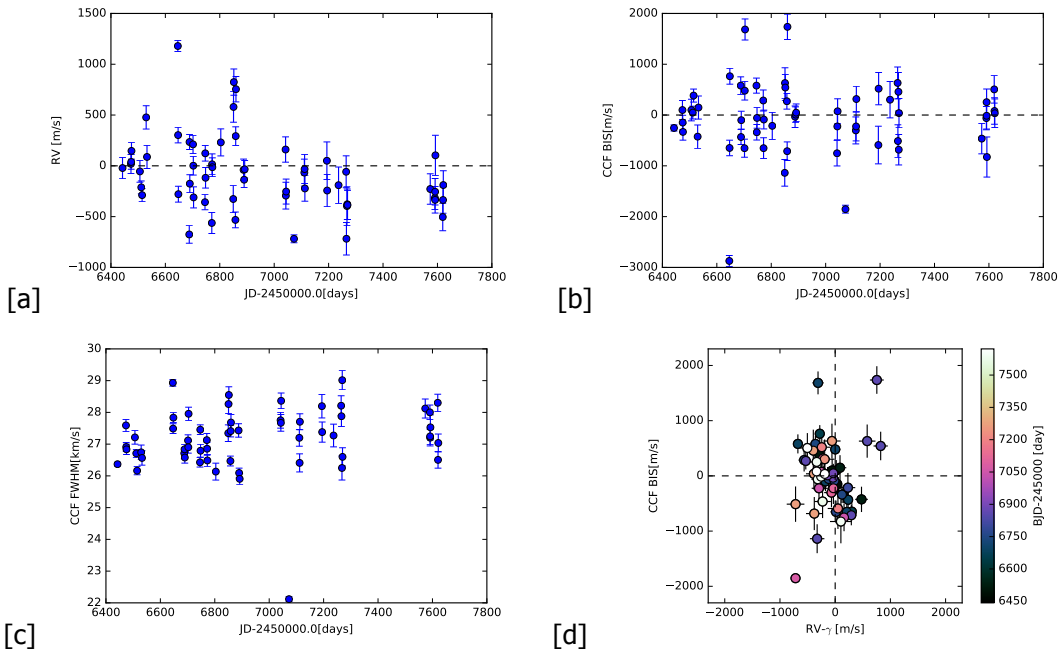

Figure 8.1: (a) represents the variation of RV of J1407 with time. (b) represents the FWHM of the star implying heavy stellar activity. (c) representing slope of bisector also is inline with the FWHM, implying high stellar activity. (d) represents the RV vs slope of bisector plot showing very high anti correlation.

$$\chi^2 = \left(\frac{(X_{obs} - X_{Model})}{\sigma} \right)^2 \tag{8.1}$$

Where,

X_{obs} represents the RV data taken at certain epochs,

X_{Model} represents the Radial Velocity obtained by the model at the respective epoch and

σ represents the value of standard deviation of the respective data.

An algorithm is created to create a model for the secondary that provides the radial velocity of the secondary at the respective epochs at which original observations were taken. The model is tested and verified with the results from kenworthy et al(2015)[11] and the results have been included in the **Appendix 11.1**. **Figure 8.2** (bottom) represents results from previous research paper by kenworthy et al.(2015)[11] and the top figure represents the algorithm generated RV constraint plot for circular orbits obtained with the new RV data. From the figure it is evident that previously 9 year orbital period was poorly constrained, whereas it is well constrained in the new result. The similarity between both the plots is that both of them are poorly constrained for orbital periods which are greater than 20 years.

Figure 8.2: RV Constraints for circular orbit

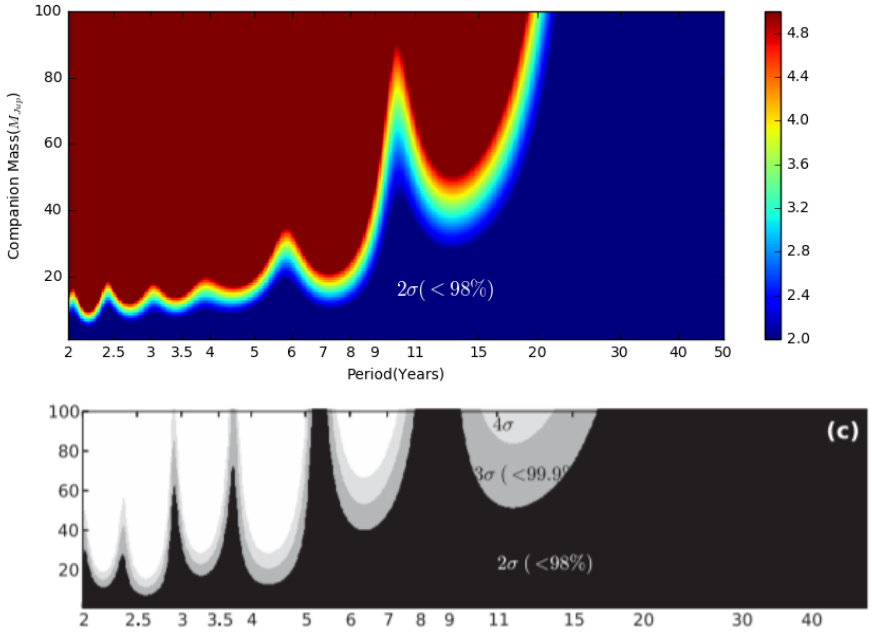

8.3. Constraints for Elliptical Orbit

Figure 8.3 represents results from previous research paper by kenworthy et al.(2015)[11] which implies that the radial velocity data yields poor constraint on all orbital periods greater than 11 years. The meaning of poor constraint here implies that the chances of finding the secondary companion is the same for all possibilities of mass and respective period.

Figure 8.4 represents the RV constraints from the updated data. The RV constraints for the ω intervals between 250 and 300 degrees is represented in the plot with eccentricity and inclination constraints included from **Chapter 5**. The new RV data looks the same for all values of ω except about the 9-11 year orbital period. It implies that the probability of the secondary companion being massive increases with the value of $omega$ in the 9-11 year orbital period range.

8.4. Conclusion

The radial velocity of J1407 is prone to lot of noise because of its young age and high stellar activity in the surface of the star. Thus, the RV data constraints are measured as a chi square fit to the model. Thus it is highly recommended in future results to use Gaussian Process(GP) to eliminate the stellar noise from the data. From the **Figure 8.4**, it is visible that still the higher orbital periods of the secondary are unconstrained. However, RV has produced significant constraints for the lower orbital periods. Combination of the result with the direct imaging constraint will possibly further constrain the longer orbital periods. These combination of constraint results are explained in the next chapter.

Figure 8.3: RV Constraints for elliptical orbit from Kenworthy et al(2015)[11]

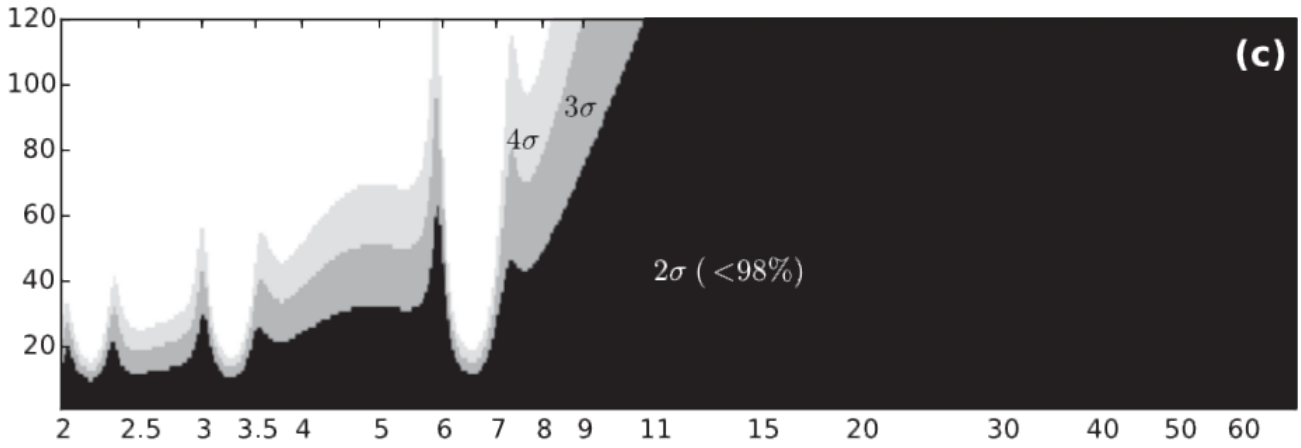

Figure 8.4: updated RV Constraints for elliptical orbit from the latest data of CORALIE observation

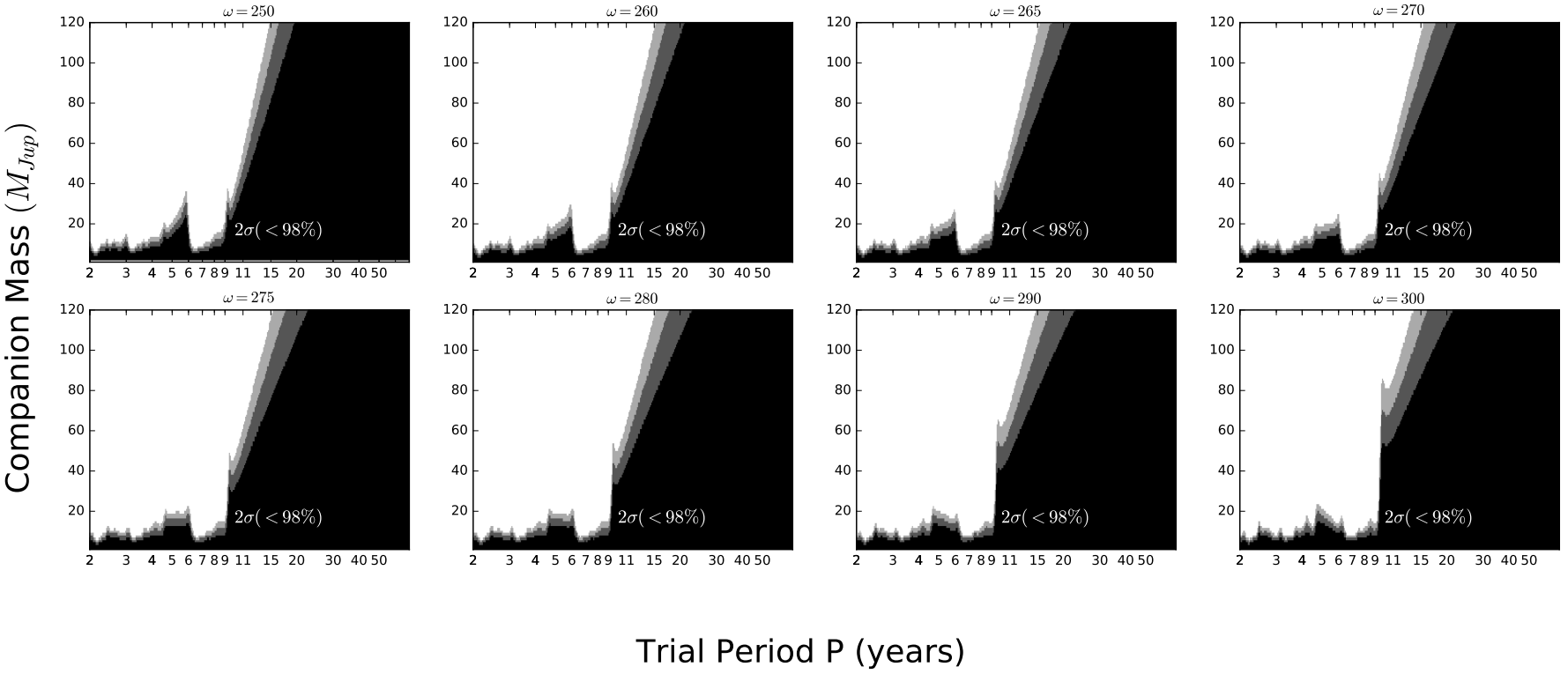

9

Results and Conclusion

9.1. Combined constraints for circular orbits

It is important to include the RV, Direct imaging, Photometry and hill sphere constraints to obtain the final result. **Figure 9.1** represent the final combined constraint for the circular orbit. The red lines indicate the ξ limit which is the ratio of the radius of the ring system to the radius of the hill sphere. ξ values greater than 0.3 can be ruled out as the ring system outside the limit are unstable for longer periods of time. The gray vertical bars represent the photometric constraint with the new data which has ruled out almost all the periods less than 10 years. The direct imaging constraint is shown by yellow region. Blue lines indicate the velocity of the secondary for that orbital period which is very less when compared to the observed velocity of 32 ±2 km s^{-1}. Thus the circular orbits can be entirely ruled out except for only one case that the ring system has clumps of materially instead of azimuthally distributed ring of particles. In that scenario, the velocity of the clump will be subtracted from the transverse velocity of J1407b leading to smaller transverse velocity and hence possibility of circular orbits with higher orbital period.

9.2. Combined constraints for elliptical orbits

Combined constraints for the elliptical orbits is shown in the **Figure 9.2** for different values of ω. It is important to note that each point in each of the plots shown in the figure has a unique value of inclination(i) and eccentricity(e) as discussed in **Chapter 5**. Earlier research papers suggested that the value of ω has to be close to 270 degrees(periastron facing the direction of observer). Thus, in that case if we assume the value of ω to be equal to 270 degrees , then the figure implies that the maximum mass that J1407b can have if we were to see the eclipse very soon will be 40 Jupiter masses. For all

Figure 9.1: Combined constraints for circular orbits

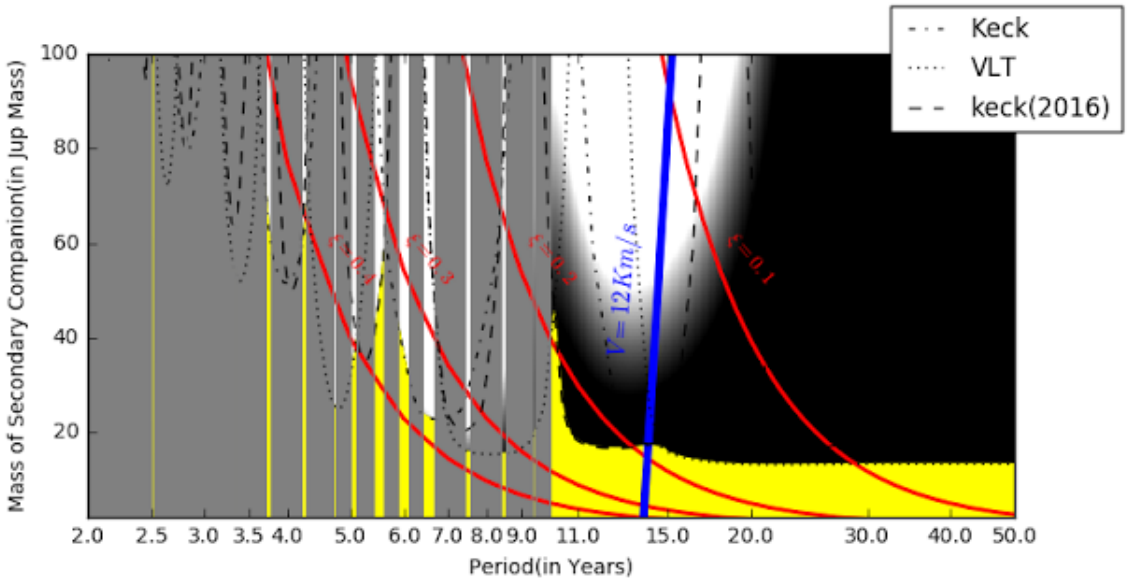

the cases considered including the worst case scenarios of $\omega = 250\ degrees$ and $\omega = 300\ degrees$, the maximum mass that J1407b can have is only about 63.5 Jupiter masses.

The extreme case of $\omega = 300\ degrees$ is only possible in case if the secondary companion has values of eccentricity greater than 0.85 which is not unusual. It would be challenging to see how the ring system will be stable in case of high eccentricities as the hill sphere of the secondary will reduce at periastron. If the secondary has orbital period of less than 12 years(most likely scenario), having had the first eclipse in April 2007, we should be able to see the eclipse in before April 2019. If it also possess the periastron direction facing the observer in earth , then J1407b is highly likely to be a brown dwarf(> 12 M_{jup}).

Table 9.1: Mean mass of J1407b for different cases of ω

ω(deg)	Mean mass of J1407b(M_J)
250	7.32
260	9.10
265	9.56
270	10.04
275	10.43
280	10.74
290	14.48
300	24.98

9.3. Result

Final constraint result from this research has still not ruled out the possibility of J1407b being a planet but has shown that the secondary can be a good possible candidate for the expanding brown dwarf catalogue. If orbital periods less than 10 years are ruled out, then from the eccentricity constraint as shown in **Chapter 5**, we can conclude that the secondary has an eccentricity value greater than 0.7 .There are only four brown dwarf candidates[51] with the eccentricity values greater than 0.7 namely(in the increasing order of eccentricity) HD 8673b[52](e=0.723), HD 219828c[53](e=0.8115), HD 22781c[54](e=0.8191) and WASP 53c[55](e=0.8369).The maximum mass of the above mentioned four brown dwarf's is around $16.35^{+0.85}_{-0.82}\ M_J$ for the WASP 53c. If the mass of J1407b is found out to be greater than 16.35 M_J, then it will become the most massive brown dwarf in a highly eccentric orbit.

Table 9.1 represents the mean mass J1407b can possess for each value of argument of periastron. The value of mean mass is derived from the **Figure 9.2**, where the possible values of mass(represented in the black region) for each period is summed and divided with the respective number of entries. The results show an increase in mean mass of J1407b with the increase in the value of ω. The reason that can be given is that , most of the higher mass regions present in the lower values of omega were at less than 10 year periods and values in less than 10 year period are ruled out by the photometry result. For example, take the case of $\omega = 300$, where most of the regions indicating the higher mass for secondary are at regions where period values are greater than 30 years. Since we have only the photometry data for the last 10 years, the respective periods are not ruled out. Hence the mean mass predicted for this particular case is very high(24.98 M_J), when compared to the other cases.

9.4. Conclusion

From this research thesis, we have successfully found the critical value of inclination which is shown in the **Figure 5.3**. In the previous research work, the values of inclination are assumed to be 90 degree and hence in this research work, the value of impact parameter is utilised to find the critical value of inclination required for particular value of ω. The value of ω was also assumed to be that of 270 degrees in the previous research work by kenworthy et al.(2015)[11]. However, in our research work we have considered possible values of ω, within a certain range,between 250 and 300 degrees, that could satisfy velocity constraints.

Thus if all the assumptions, regarding the particles in the ring system and gravitationally bound secondary, hold true, then the results produce a new insight into the mass and orbital elements of the of the secondary. If the secondary's orbit has argument of periastron to be of value equal to 300 degrees, then the maximum mass it can be of is 63.5 M_J. This produces great insight into the mass of J1407b as it completely rules out the theory of J1407b to be a more massive red dwarf(m>80 M_J).

Hence the secondary has to be a cooler brown dwarf(13-85 M_J) not having enough mass to ignite hydrogen into helium, or a gas giant planet(< 13 M_J), lying well below the deuterium fusing limit[56].

From the **Figure 9.2**, it is clear that the orbital period is poorly constrained. The plot shows that the higher orbital periods are still possible for the secondary's orbit having high eccentricities. Only way to constrain period limit is to arrange for another direct imaging observation with Keck or VLT telescope, since it can clearly rule out higher orbital periods.

Assuming orbital periods less than 10 years are completely ruled out, from the eccentricity constraints(Figure 5.1), it is clear that the secondary must have an eccentricity value equal to or greater than 0.7. For these values of high eccentricity, the companion must be very close to its parent star at the time of periastron passage. Hence , its hill sphere greatly shrinks, and hence it is highly probable that the outer particles in the ring system must be greatly perturbed by the gravity of its parent star. Thus the secondary might have lost some of its particles in the ring system. Thus the amount of particles blocking the star light changes and hence, we may expect a different set of observational transit data during the next eclipse. Nevertheless, the change may not be very large and hence we can expect another long eclipse with a change in depth of transit.

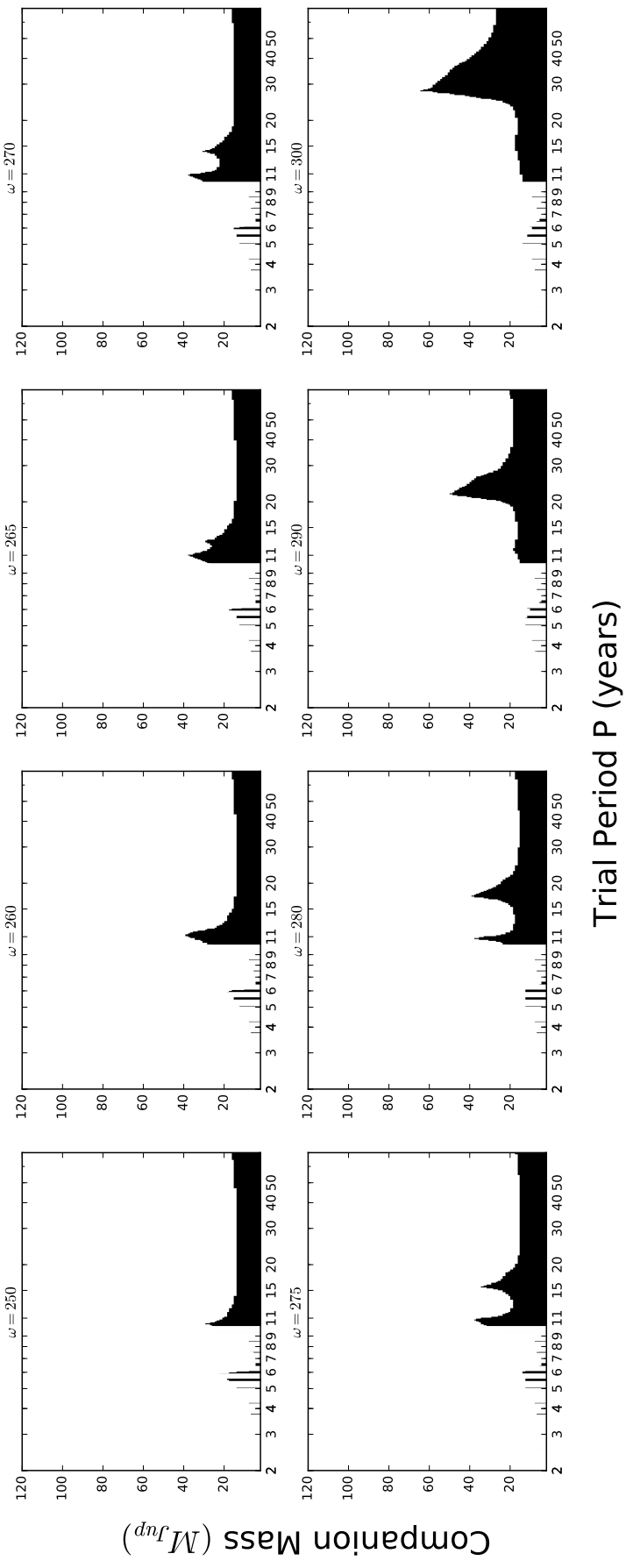

Figure 9.2: Combined constraints of RV, DI and photometry for elliptical orbits. The Mean mass for each case of ω(in increasing order) are 7.32,9.10,9.56,10.04,10.43,1.74,14.48 and 24.98 Jupiter masses respectively.

10

Recommendations

Future course of work to solve the problem related to J1407b is discussed in this chapter.

A Rogue companion?

What if the secondary is a rogue companion?. If the companion is not bound to its star, then neither the period limit shown as the result nor the elliptical orbit theory will make any sense. The possible recommendation if the above mentioned case is true is that, researchers can calculate the separation of J1407 from 2007(as it would move in a straight line if it is not bound to its parent star) and view the particular space in sub millimeter wavelength. The rings will glow in sub millimeter wavelength and hence J1407b and its rings can be detected if it is unbound to the star. If they are not detected in that particular space, we can confirm that the secondary is bound to its parent star.

Presence of clumps in the rings?

Kenworthy and Mamajek(2014)[3] assumed azimuthally uniform distribution of particles in the ring system and developed their model for the ring system. Thus the particles in the ring system does not contribute to the velocity of the secondary in the observation. Hence the observed velocity of 32 ±2 kms^{-1} is assumed to be the velocity of the secondary alone and we have developed our constraints. However, in case of presence of clumps in the ring system, the clumps will contribute to the velocity observed and hence the assumed velocity of the secondary might not be as high as 32 kms^{-1}. Thus even circular orbits cannot be ruled out in that case and hence our results will also become invalid. Modelling random clumps in the disk are highly impractical and hence that option can be ruled out. As

stated earlier, next eclipse for the PDS 110 system (introduced in **Chapter 7**) is expected on September 2017. Since, it is also orbiting a young star, the exoplanet is also assumed to be young and the additional spectroscopic data from the light reflected from the rings will shed light into the science of nature of particles in its ring system. Researcher's have already modelled the orientation and the geometry of the ring system. Hence, the additional data will confirm the ring model and the proposed symmetric distribution of particles in the ring system.

Noise in RV

J1407 is very similar to PDS 110 system because of high stellar activity. At least we know the period of the secondary in the PDS 110 system. But in case of J1407, both the period and mass constraints are still open to wide range of values. Since RV consists of lot of noise due to the stellar activity, a good possible solution to the problem is using the Gaussian Process[57] which utilises the covariance between the two data points to remove the noise cause due to the stellar noise.

New Direct Imaging Observation

Another recommendation would be to make use of the direct imaging technique. Its because, transit and direct imaging are the only left out techniques to observe J1407 because of the noise measurements in RV. Transit data can confirm J1407b only when it appears again to the observer. One night of observation at Keck can solve this problem as it can further rule out particular regions of mass and period.

11

Appendix

11.1. Appendix-a

The algorithm to model the radial velocity of the star has been created. The function of the algorithm is to calculate the radial velocity of the star caused by the secondary at the same epochs of time as given in the RV data.

The **Figure 11.1** represents the RV constraints published in the paper kenworthy et al.(2015)[11]. In the paper, they have produced this result for $\omega = 270$, i=90 and e=0. However, there has been a critical mistake in the assumption of the orbital parameters and also the degree of freedom(n). The no. of constraints used is only one which is a straight line fit to the model. They are explained in the below equation.

$$degree\ of\ freedom(n) = no.\ of\ data\ points - no.\ of\ constraints - 1 \tag{11.1}$$

The author has calculated this result for $\omega = 90$ instead of required $\omega = 270$. This can be proved with the help of **Figure 11.2**, which is the output of the algorithm for $\omega = 90$ and n=7. Both the figures match each other and hence our algorithm has been verified. However it is important to produce the result for the right orbital parameter of $\omega = 270$ and n=11 which is produced in the **Figure 11.3**.

11.2. Appendix-b

This section explains the result of our newly developed algorithm for the direct imaging technique. **Figure 11.4**(top) explains the separation of the secondary in (arc seconds) in the sky for different orbital periods and (bottom) explains the converted separation limit to the mass limit of the secondary for the respective separation. The yellow region indicates the probable mass the secondary can have for

Figure 11.1: RV constraint for circular orbits[11]

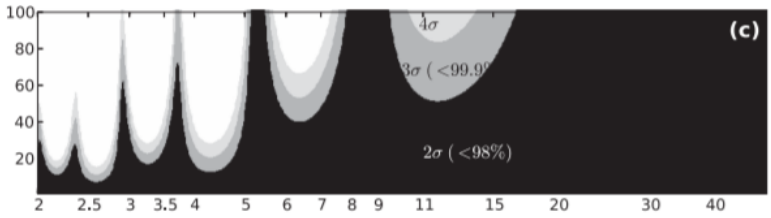

Figure 11.2: RV constraint result $\omega = 90$ and n=9

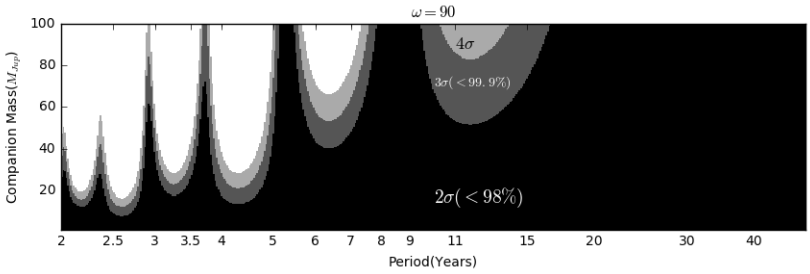

Figure 11.3: RV constraint result $\omega = 270$ and n=11

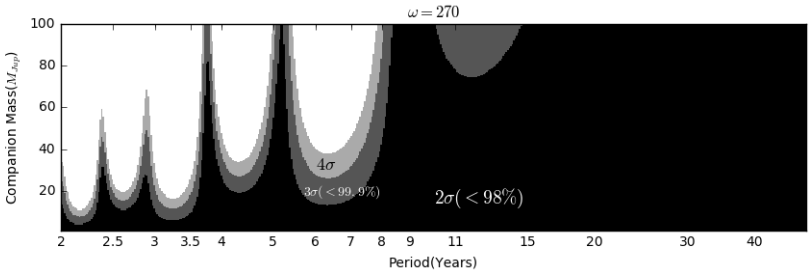

the particular orbital period. The result expressed in the **Figure 11.4** is same as the result published in the paper Kenworthy et al.2015[11], represented in the **Figure 11.5**. Hence our algorithm is verified.

Figure 11.4: Direct imaging result for circular orbits

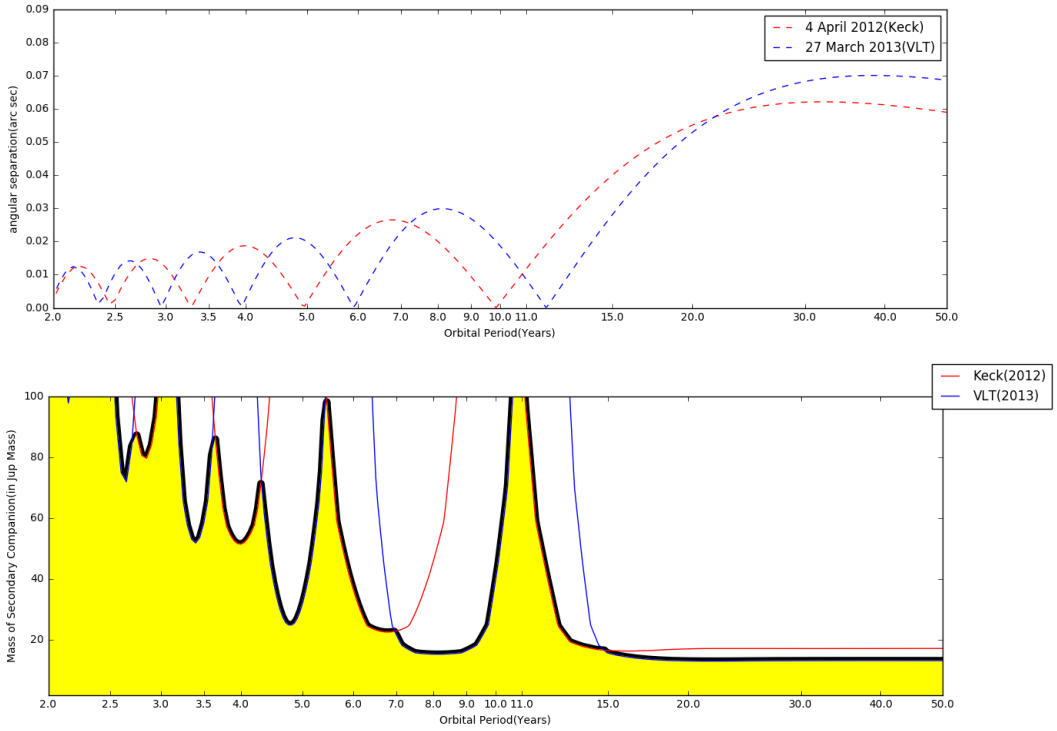

Figure 11.5: Direct imaging constraint[11]

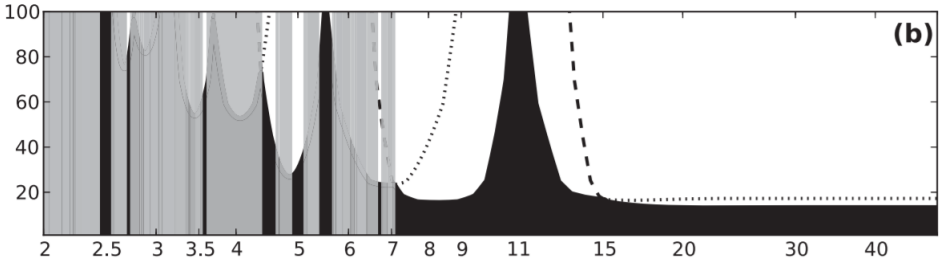

Bibliography

[1] *Habitable zone around the nearest star,* https://www.nasa.gov/feature/jpl/eso-discovers-earth-size-planet-in-habitable-zone-of-nearest-star, accessed: 20th June 2017.

[2] *Anatomy of planetary transit,* http://www.planetary.org/multimedia/space-images/charts/anatomy-of-a-planetary.html, accessed: 3rd July 2017.

[3] M. A. Kenworthy and E. E. Mamajek, *Modeling giant extrasolar ring systems in eclipse and the case of j1407b: sculpting by exomoons?* The Astrophysical Journal **800**, 126 (2015).

[4] *Gigantic ring system around J1407b,* http://www.rochester.edu/newscenter/gigantic-ring-system-around-j1407b/, accessed: 20th June 2017.

[5] W. Borucki, D. Koch, J. Jenkins, D. Sasselov, R. Gilliland, N. Batalha, D. Latham, D. Caldwell, G. Basri, T. Brown, *et al.*, *Kepler's optical phase curve of the exoplanet hat-p-7b,* Science **325**, 709 (2009).

[6] *Radial velocity Method,* https://adlerastrojournalists.wordpress.com/category/astrobiology/page/3/, accessed: 3rd July 2017.

[7] *Direct Imaging and its exoplanetary uses,* https://www.centauri-dreams.org/?p=3195, accessed: 4th July 2017.

[8] *Open Exoplanet Catalogue,* http://www.openexoplanetcatalogue.com/, accessed: 16th June 2017.

[9] E. E. Mamajek, A. C. Quillen, M. J. Pecaut, F. Moolekamp, E. L. Scott, M. A. Kenworthy, A. C. Cameron, and N. R. Parley, *Planetary construction zones in occultation: discovery of an extrasolar ring system transiting a young sun-like star and future prospects for detecting eclipses by circumsecondary and circumplanetary disks,* The Astronomical Journal **143**, 72 (2012).

[10] S. Rieder and M. A. Kenworthy, *Constraints on the size and dynamics of the j1407b ring system,* Astronomy & Astrophysics **596**, A9 (2016).

[11] M. Kenworthy, E. Mamajek, S. Lacour, A. Kraus, H. Triaud, E. Scott, D. Segransan, M. Ireland, F. Hambsch, D. Reichart, J. Haislip, A. LaCluyze, J. Moore, and N. Frank, *Mass and Period limits on the ringed companion transiting the young star J1407,* Monthly Notices of the Royal Astronomical Society **446** (2015).

[12] C. Marois, B. Macintosh, T. Barman, B. Zuckerman, I. Song, J. Patience, D. Lafrenière, and R. Doyon, *Direct imaging of multiple planets orbiting the star hr 8799,* Science **322**, 1348 (2008).

[13] *Venus Transit Path | NASA,* https://www.nasa.gov/mission_pages/sunearth/news/gallery/venustransit-path.html, accessed: 10th June 2017.

[14] J. N. Winn, *Transits and occultations,* arXiv preprint arXiv:1001.2010 (2010).

[15] *Detection of exoplanets,* http://www.markelowitz.com/Exoplanets.html, accessed: 14th June 2017.

[16] T. Van Werkhoven, M. Kenworthy, and E. Mamajek, *Analysis of 1swasp j140747. 93- 394542.6 eclipse fine-structure: hints of exomoons,* Monthly Notices of the Royal Astronomical Society **441**, 2845 (2014).

[17] H. Osborn, J. Rodriguez, M. Kenworthy, G. Kennedy, E. Mamajek, C. Robinson, C. Espaillat, D. Armstrong, B. Shappee, A. Bieryla, *et al.*, *Periodic eclipses of the young star pds 110 discovered with wasp and kelt photometry,* Monthly Notices of the Royal Astronomical Society , stx1249 (2017).

[18] *The All Sky Automated Survey,* http://www.astrouw.edu.pl/asas/, accessed: 14th June 2017.

[19] M. Mayor and D. Queloz, *A jupiter-mass companion to a solar-type star,* (1995).

[20] D. Lafrenière, R. Jayawardhana, and M. H. Van Kerkwijk, *The directly imaged planet around the young solar analog 1rxs j160929. 1–210524: Confirmation of common proper motion, temperature, and mass,* The Astrophysical Journal **719**, 497 (2010).

[21] M. Gillon, A. H. Triaud, B.-O. Demory, E. Jehin, E. Agol, K. M. Deck, S. M. Lederer, J. De Wit, A. Burdanov, J. G. Ingalls, *et al.*, *Seven temperate terrestrial planets around the nearby ultracool dwarf star trappist-1,* Nature **542**, 456 (2017).

[22] J. Maız-Apellaniz, *The Origin of Local Bubble,* The Astrophysical Journal (2001).

[23] M. Pecaut, E. Mamajek, and E. Bubar, *A Revised Age for Upper Scorpius and The Star-Formation History Among the F-Type Members of the Scorpius-Centaurus OB Association,* The Astrophysical Journal (2011).

[24] N. Zacharias, C. Finch, and T. Girard, *The Third US Naval Observatory CCD Astrograph catalog (UCAC3),* The Astronomical Journal (2010).

[25] P. C. Keenan and R. C. McNeil, *The perkins catalog of revised mk types for the cooler stars,* The Astrophysical Journal Supplement Series **71**, 245 (1989).

[26] *superwasp-wide angle search for planets,* http://www.superwasp.org/, accessed: 7th May 2017.

[27] E. E. Mamajek and L. A. Hillenbrand, *Improved age estimation for solar-type dwarfs using activity-rotation diagnostics,* The Astrophysical Journal **687**, 1264 (2008).

[28] W. Herbst, K. LeDuc, C. M. Hamilton, J. N. Winn, M. Ibrahimov, R. Mundt, and C. M. Johns-Krull, *The light curve of the weakly accreting t tauri binary kh 15d from 2005-2010: Insights into the nature of its protoplanetary disk,* The Astronomical Journal **140**, 2025 (2010).

[29] V. Grinin, H. Stempels, G. F. Gahm, S. Sergeev, A. Arkharov, O. Barsunova, and L. Tambovtseva, *The unusual pre-main-sequence star v718 persei (hmw 15)-photometry and spectroscopy across the eclipse,* Astronomy & Astrophysics **489**, 1233 (2008).

[30] *Very Large Telescope,* http://www.eso.org/public/teles-instr/paranal-observatory/vlt/, accessed: 29th May 2017.

[31] *Keck telescope,* http://www.keckobservatory.org/, accessed: 29th May 2017.

[32] F. Allard, D. Homeier, and B. Freytag, *Models of very-low-mass stars, brown dwarfs and exoplanets,* Phil. Trans. R. Soc. A **370**, 2765 (2012).

[33] D. Reichart, M. Nysewander, J. Moran, J. Bartelme, M. Bayliss, A. Foster, J. C. Clemens, P. Price, C. Evans, J. Salmonson, *et al.*, *Prompt: panchromatic robotic optical monitoring and polarimetry telescopes,* arXiv preprint astro-ph/0502429 (2005).

[34] F.-J. Hambsch, *Road (remote observatory atacama desert): intensive observations of variable stars,* in *Society for Astronomical Sciences Annual Symposium*, Vol. 31 (2012) pp. 75–78.

[35] R. Bernstein, S. A. Shectman, S. M. Gunnels, S. Mochnacki, and A. E. Athey, *Mike: a double echelle spectrograph for the magellan telescopes at las campanas observatory,* in *Astronomical Telescopes and Instrumentation* (International Society for Optics and Photonics, 2003) pp. 1694–1704.

[36] D. Queloz, M. Mayor, S. Udry, M. Burnet, F. Carrier, A. Eggenberger, D. Naef, N. Santos, F. Pepe, G. Rupprecht, *et al.*, *From coralie to harps. the way towards 1 m s-1 precision doppler measurements,* The Messenger **105**, 1 (2001).

[37] R. G. Martin and S. H. Lubow, *Tidal truncation of circumplanetary discs,* Monthly Notices of the Royal Astronomical Society **413**, 1447 (2011).

[38] A. Quillen and D. Trilling, *Do proto-jovian planets drive outflows?* The Astrophysical Journal **508**, 707 (1998).

[39] M. C. Liu, E. A. Magnier, N. R. Deacon, K. N. Allers, T. J. Dupuy, M. C. Kotson, K. M. Aller, W. Burgett, K. Chambers, P. Draper, *et al.*, *The extremely red, young l dwarf pso j318. 5338–22.8603: a free-floating planetary-mass analog to directly imaged young gas-giant planets,* The Astrophysical Journal Letters **777**, L20 (2013).

[40] C. Marois, D. Lafreniere, R. Doyon, B. Macintosh, and D. Nadeau, *Angular differential imaging: A powerful high-contrast imaging techniquebased on observations obtained at the gemini observatory, which is operated by the association of universities for research in astronomy, inc., under a cooperative agreement with the nsf on behalf of the gemini partnership: the national science foundation (united states), the particle physics and astronomy research council (united kingdom), the national research council (canada), conicyt (chile), the australian research council (australia), cnpq (brazil), and conicet (argentina).* The Astrophysical Journal **641**, 556 (2006).

[41] D. Lafreniere, C. Marois, R. Doyon, D. Nadeau, and E. Artigau, *A new algorithm for point-spread function subtraction in high-contrast imaging: A demonstration with angular differential imaging,* The Astrophysical Journal **660**, 770 (2007).

[42] P. L. Wizinowich, D. Le Mignant, A. H. Bouchez, R. D. Campbell, J. C. Chin, A. R. Contos, M. A. van Dam, S. K. Hartman, E. M. Johansson, R. E. Lafon, *et al.*, *The wm keck observatory laser guide star adaptive optics system: overview,* Publications of the Astronomical Society of the Pacific **118**, 297 (2006).

[43] *MEarth-North Observatory,* https://www.cfa.harvard.edu/MEarth/Telescopes.html, accessed: 16th June 2017.

[44] *Kepler & K2,* https://keplerscience.arc.nasa.gov/objectives.html, accessed: 16th June 2017.

[45] *CoRoT,* http://sci.esa.int/corot/, accessed: 16th June 2017.

[46] D. Stam, *Spectropolarimetric signatures of earth-like extrasolar planets,* Astronomy & Astrophysics **482**, 989 (2008).

[47] A. Santerne, R. Díaz, C. Moutou, F. Bouchy, G. Hébrard, J.-M. Almenara, A. Bonomo, M. Deleuil, and N. Santos, *Sophie velocimetry of kepler transit candidates-vii. a false-positive rate of 35% for kepler close-in giant candidates,* Astronomy & Astrophysics **545**, A76 (2012).

[48] T. van Werkhoven, M. Kenworthy, and E. Mamajek, *Analysis of 1SWASP J140747.93−394542.6 eclipse fine-structure: hints of exomoons,* Monthly Notices of the Royal Astronomical Society **441** (2014).

[49] D. Queloz, M. Mayor, L. Weber, A. Blécha, M. Burnet, B. Confino, D. Naef, F. Pepe, N. Santos, and S. Udry, *The coralie survey for southern extra-solar planets. i. a planet orbiting the star gliese 86,* A&A **354**, 99 (2000).

[50] D. Ségransan, S. Udry, M. Mayor, D. Naef, F. Pepe, D. Queloz, N. Santos, B.-O. Demory, P. Figueira, M. Gillon, *et al.*, *The coralie survey for southern extrasolar planets-xvi. discovery of a planetary system around hd 147018 and of two long period and massive planets orbiting hd 171238 and hd 204313,* A&A **511**, A45 (2010).

[51] *NASA Exoplanet Archive,* https://exoplanetarchive.ipac.caltech.edu/, accessed: 18th June 2017.

[52] L. C. Roberts Jr, B. D. Mason, C. R. Neyman, Y. Wu, R. L. Riddle, J. C. Shelton, J. Angione, C. Baranec, A. Bouchez, K. Bui, *et al.*, *Know the star, know the planet. iv. a stellar companion to the host star of the eccentric exoplanet hd 8673b,* The Astronomical Journal **149**, 144 (2015).

[53] N. Santos, A. Santerne, J. Faria, J. Rey, A. Correia, J. Laskar, S. Udry, V. Adibekyan, F. Bouchy, E. Delgado-Mena, *et al.*, *An extreme planetary system around hd 219828-one long-period super jupiter to a hot-neptune host star,* Astronomy & Astrophysics **592**, A13 (2016).

[54] R. Díaz, A. Santerne, J. Sahlmann, G. Hébrard, A. Eggenberger, N. Santos, C. Moutou, L. Arnold, I. Boisse, X. Bonfils, *et al.*, *The sophie search for northern extrasolar planets-iv. massive companions in the planet-brown dwarf boundary,* Astronomy & Astrophysics **538**, A113 (2012).

[55] A. H. Triaud, M. Neveu-VanMalle, M. Lendl, D. R. Anderson, A. Collier Cameron, L. Delrez, A. Doyle, M. Gillon, C. Hellier, E. Jehin, *et al.*, *Peculiar architectures for the wasp-53 and wasp-81 planet-hosting systems□,* Monthly Notices of the Royal Astronomical Society **467**, 1714 (2017).

[56] D. S. Spiegel, A. Burrows, and J. A. Milsom, *The deuterium-burning mass limit for brown dwarfs and giant planets,* The Astrophysical Journal **727**, 57 (2011).

[57] V. Rajpaul, S. Aigrain, M. A. Osborne, S. Reece, and S. Roberts, *A gaussian process framework for modelling stellar activity signals in radial velocity data,* Monthly Notices of the Royal Astronomical Society **452**, 2269 (2015).